Rational design of photochromic analogs of tricyclic drugs

Fabio Riefolo,[1,2,†] Rosalba Sortino,[1,2,‡] Carlo Matera,[1,2,3,‡] Enrique Claro,[4] Beatrice Preda,[1] Simone Vitiello,[1,¤] Sara Traserra,[5] Marcel Jiménez,[5,6] Pau Gorostiza[1,2,7,]*

[1] Institute for Bioengineering of Catalonia (IBEC), Barcelona Institute for Science and Technology (BIST), Barcelona 08028, Spain.

[2] Network Biomedical Research Center in Bioengineering, Biomaterials, and Nanomedicine (CIBER-BBN), Madrid 28029, Spain.

[3] Department of Pharmaceutical Sciences, University of Milan, Milan 20133, Italy.

[4] Institut de Neurociències and Departament de Bioquímica i Biologia Molecular, Unitat de Bioquímica de Medicina, Universitat Autònoma de Barcelona (UAB), Barcelona 08193, Spain.

[5] Department of Cell Biology, Physiology and Immunology, Universitat Autonoma de Barcelona, Barcelona 08193, Spain.

[6] Centro de Investigación Biomédica en Red de Enfermedades Hepáticas y Digestivas (CIBERehd), Instituto de Salud Carlos III, Madrid 28029, Spain.

[7] Catalan Institution for Research and Advanced Studies (ICREA), Barcelona 08010, Spain.

Muscarinic Acetylcholine Receptors, Photopharmacology, Pirenzepine, Crypto-azologizations, Antagonists, Photochromism, Photoswitch, Azobenzene, Light, G protein-coupled receptor, GPCR, Optopharmacology, Azologization, Caged compound, Optogenetics.

ABSTRACT

Tricyclic chemical structures are the core of many important drugs targeting all neurotransmitter pathways. These medicines enable effective therapies to treat from peptic ulcer disease to psychiatric disorders. However, when administered systemically they cause serious adverse effects that limit their use. In order to obtain localized and on-demand pharmacological action using light, we have designed photoisomerizable ligands based on azobenzene that mimic the tricyclic chemical structure and display reversibly controlled activity. Pseudo analogs of the tricyclic antagonist pirenzepine demonstrate that this is an effective strategy in muscarinic acetylcholine receptors, showing stronger inhibition upon illumination both *in vitro* and in cardiac atria *ex vivo*. Despite the applied chemical modifications to make pirenzepine derivatives sensitive to light stimuli, the most potent candidate of the set, cryptozepine-**2,** maintained a moderate but promising M1 *vs* M2 subtype selectivity. These photoswitchable “crypto-azologs” of tricyclic drugs might open a general way to spatiotemporally target their therapeutic action while reducing their systemic toxicity and adverse effects.

INTRODUCTION

Photopharmacology is a modern branch of pharmacology that aims to improve the efficacy and safety of drugs by directing their action to target organs and controlling their doses using light. It deals with molecular strategies to photo-regulate drug activity.[1,2] Most photoswitchable small molecule ligands developed in recent years have exploited the reduced size and robust photochromism of azobenzene, which allows two design approaches: (1) tailoring compounds through extension of the drug core ("azo-extension" approach), and (2) introducing an isosteric azobenzene photoswitch in the core ("azologization" approach).[3,4] The latter is the most straightforward design strategy and is generally preferred because it requires minimal modifications of the original structure, thus maintaining the drug-likeness of the parent compound and largely preserving its pharmacokinetic and pharmacodynamic properties.[5,6] If azologization motifs are not present, in some cases the drug structure can be extended with a photoswitchable moiety while retaining the drug activity.[3,7] However, these versatile and complementary strategies are not applicable to all drugs. This is often the case when azobenzene-like motifs are absent from a parent molecule that can only tolerate minor variations in size (i.e., non-azologizable and non- azo-extendable drugs), thus hampering the reach of photopharmacology. An important class of drugs that has not been endowed with photo-regulation is characterized by the general formula of **Figure 1A**, i.e. those fused tricyclic compounds which are known as "privileged structures" in medicinal chemistry.[8] This term was coined by Ben Evans in 1988 to recognize the potential of certain structural motifs as templates for derivatization and discovery of novel biological ligands.[9] A great diversity of tricyclic derivatives has been developed and are marketed for different clinical conditions. They include central nervous system agents such as tricyclic antidepressants used to treat psychiatric disorders[10] but also for other therapeutic indications such as loratadine (an antihistamine drug used to treat the symptoms of allergies), nevirapine (a non-competitive HIV-1 reverse transcriptase inhibitor), lonafarnib (a farnesyl transferase inhibitor used as anticancer), and pirenzepine (an antimuscarinic drug to treat peptic ulcers).[11]

An arylazo moiety (e.g., an azobenzene) in its *cis* configuration can quite resemble (at least in some of its conformations) the geometry of the tricyclic scaffold, whereas the corresponding *trans* isomer cannot. This is illustrated by the three-dimensional alignment of conformers in **Figure 1B**. Thus, we devised a way to mimic the tricyclic system of these drugs with a photochromic arylazo unit by means of two modifications: (1) the isosteric substitution of the two-atom bridge connecting the aryl rings with a –N=N– group to confer photochromic behavior, and (2) the cleavage (ring opening) of one of the two single bonds forming the one-atom bridge, to increase the flexibility and to enable greater changes in geometry upon photoisomerization. In this way, the photochromic pseudo-analog of the tricyclic drug should be able to maintain the pharmacological properties of the parent compound upon photoisomerization to the *cis* configuration. Conversely, the most thermodynamically stable *trans* isomer should display a reduced capacity to modulate its biological target. This situation would be particularly favorable to apply the inactive drug in the absence of illumination and to photoactivate it at the desired locations and times. We named this novel procedure to design photoswitchable small molecules "crypto-azologization" (where the prefix "crypto-" comes from the Ancient Greek word κρυπτός [kruptós], meaning "hidden") because it expands the azologization strategy to compounds in which the potential photochromic scaffold is buried and must be sculpted out of the parent structure by a ring opening in addition to the canonical azosteric replacement.

As a test bed for our design strategy, we chose the muscarinic acetylcholine receptor (mAChR) antagonist pirenzepine (**Figure 1C**) both because of its tricyclic structure and therapeutic importance. Muscarinic receptors belong to the class A family of G-protein-coupled receptors (GPCRs) and are classified in five distinct subtypes.[12,13] The wide distribution of mAChRs in the body and the limited subtype selectivity of muscarinic drugs are the cause of their adverse effects, which have made these receptors an attractive target in photopharmacology.[14–16] Pirenzepine (Gastrozepine) is an M1-selective muscarinic antagonist marketed to treat peptic ulcers. In particular, it inhibits the parasympathetic nervous system "rest-and-digest" response, reducing gastric acid secretion and

muscle spasm.[17–20] Other potential applications have been considered, like slowing down myopia progression[21] and reducing the risk of lethal events in the ischemic heart disease.[22] The wide expression of M_1 mAChRs in the hippocampus and medial prefrontal cortex suggests that M_1-mediated signaling is important for cognitive and learning functions and plays a key role in several neurological disorders.[12,13] The development of photoswitchable M_1 ligands is thus of great interest both for therapeutic and research purposes. Here, we report the synthesis of photoswitchable M_1 mAChR antagonists designed by crypto-azologization of pirenzepine, and the characterization of their photopharmacological effects *in vitro* and *ex vivo.*

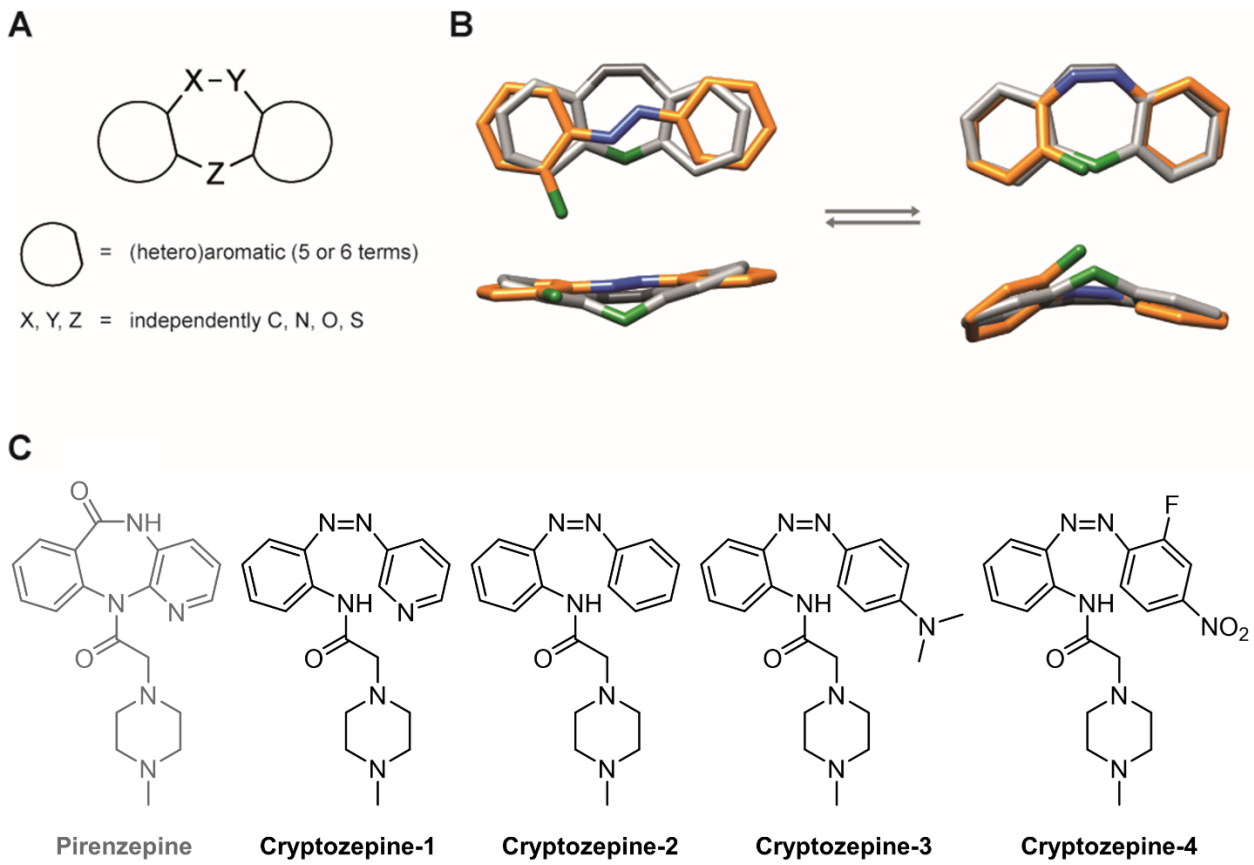

Figure 1. Design strategy and structure of crypto-azologs. (**A**) General scaffold of fused tricyclic drugs. (**B**) Best three-dimensional alignment of an azobenzene scaffold (*trans* on the left and *cis* on the right, both in orange) over a generic fused tricyclic system (in gray). For the sake of comparison, the carbon atom of the 1-atom bridge of the tricyclic system

and the corresponding carbon atom of the azobenzene are indicated in green. Nitrogen atoms are in blue. (**C**) Chemical structure of the muscarinic M_1 antagonist pirenzepine and the cryptozepines, the photochromic derivatives discussed in this work.

RESULTS AND DISCUSSION

Rational Design and Chemical Synthesis. As an initial control for our design strategy, we performed docking simulations of a representative structure at the M1 mAChR.[23] The results supported our hypothesis (see **SI** for details) and encouraged us to pursue the synthesis of a small set of pirenzepine crypto-azologs that were named "cryptozepines" (**Figure 1C**). Previous studies on pirenzepine congeners have shown how the nature and placement of accessory groups on the central core of the molecule determine the differences in receptor recognition and the binding process at mAChRs.[19] In particular, the positioning of the protonated nitrogen atom at the end of the piperazine, that is affected by the geometry of the whole structure, is crucial for the receptor recognition and the binding processes in M_1 mAChRs.[19,23,24] On the other hand, certain structural modifications at the tricyclic core are tolerated. The endocyclic amide group is thought to participate in polar interactions at the binding site, therefore its replacement with a lipophilic function such as an ethylene bridge would likely produce a loss of affinity, whereas an azo group could be better accepted. The exocyclic amide group and the nitrogen atom in one of the two aromatic rings seem to have only a minor effect in terms of affinity and selectivity.[19] As such, we decided to conserve the essential 2-(4-methylpiperazin-1-yl)acetamide side chain in all the novel derivatives, while the endocyclic amide group was replaced with an azo group and the central 7-membered ring was "opened" to generate a fully unconstrained photochromic unit. In addition, structural variations at this unit were rationally designed in order to obtain analogs endowed with different photochemical properties. Cryptozepine-**1** and cryptozepine-**2** are straightforward crypto-azologs of pirenzepine and differ from one another in the presence of the nitrogen atom in one of the two aromatic rings of Criptozepine-**1**. This feature

should significantly reduce the half-life of thermal relaxation of the *cis* isomer, as well as an increase in the aqueous solubility of this derivative. We expected though that these two derivatives would need ultraviolet (UV) light to undergo *trans*-to-*cis* isomerization, which is generally not convenient in biology.[25] Cryptozepine-**3** was designed to overcome this limitation by introducing an electron-donating group ($-NMe_2$) at the *para* position of the benzene ring which is not directly connected to the side chain, in order to produce a red-shifting "push−pull" effect (**Figure 1C**).[26] A fourth compound, Cryptozepine-**4**, characterized by a different "push-pull" system was designed and prepared, but because of its very low aqueous solubility at neutral pH we could not test its pharmacological properties. However, its physicochemical characterization is reported in the SI.

As mentioned above, we hypothesized that the M_1 mAChR should be able to properly accommodate the new ligands in their *cis* configuration, while the *trans* geometry should hinder the rest of the molecule from entering the binding pocket. Cryptozepines **1**, **2** and **3** were synthesized as illustrated in **Scheme 1**. *N*-Chloroacetyl-2-nitroaniline was reduced to the corresponding amine (**5**) by treatment with iron in ammonium chloride and acetic acid. Oxidation with Oxone® gave the nitroso derivative (**6**), which was then coupled to the chosen arylamine under Mills conditions to yield the arylazo intermediates (**7a**, **7b**, **7c**). Nucleophilic substitution of the chlorine with 1-methylpiperazine and subsequent treatment with hydrochloric acid afforded the three final compounds as dihydrochloride salts (**1**, **2**, **3**). To synthesize Cryptozepine-**4** (**Scheme 1**), 2-fluoro-4-nitroaniline was oxidized with Oxone® to give the nitroso derivative (**8**), which was then coupled to the corresponding amine (**5**) under Mills conditions to yield the arylazo intermediate (**9**). Nucleophilic substitution of the chlorine with 1-methylpiperazine afforded the Cryptozepine-**4**.

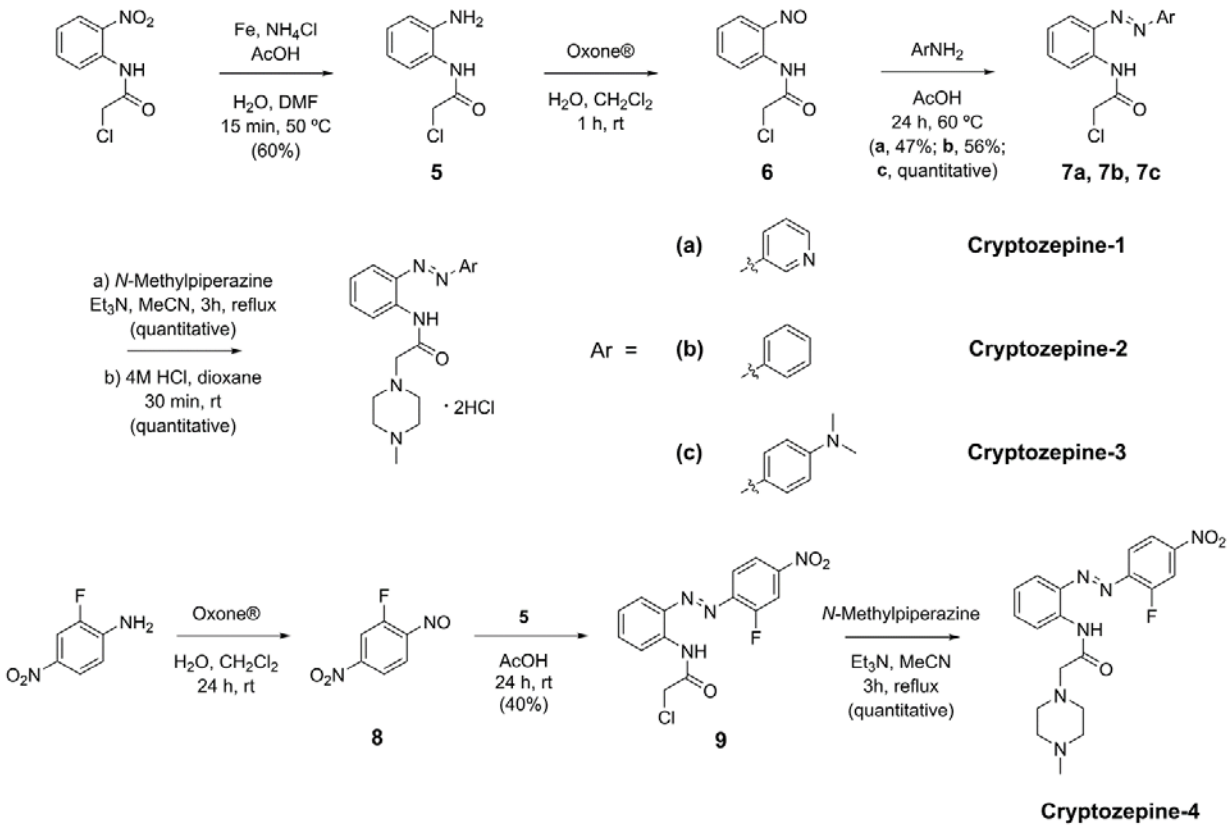

Scheme 1. The chemical synthesis of cryptozepines.

Photochemical Characterization. We then tested the ability of our photoswitchable compounds to effectively respond to light. First, we characterized the three cryptozepines by UV-Vis spectroscopy. Cryptozepines **1** and **2** displayed a clear photochromic behavior and the typical absorption bands of azobenzenes in water, with maxima at 318 nm and 433 nm due to the π–π* and n–π* transitions, respectively (**Figure 2** and **SI**). As expected, the presence of an electron-donating group in cryptozepine-**3** resulted in a strong red-shift of the π–π* transition band, with an absorption maximum at 465 nm in aqueous solution. In this case, it was not possible to observe any change in the absorption spectrum with steady-state spectroscopy in aqueous solution since the thermal isomerization of this kind of azobenzenes in protic solvents occurs extremely fast and generally completes within milliseconds.[27] However, we proved the capacity of compound **3** to photoisomerize in a dry organic solvent (**Figure 2** and **SI**). We then determined the photostationary distribution of cryptozepines **1**

and **2** by ^{1}H-NMR analysis. The distribution changed from about 90% in favor of the *trans* form in the dark to about 10% (90% in favor of the *cis* form) after illumination with UV light (365 nm) for both compounds. Compounds **1** and **2** also showed a good thermal stability, with a half-life of thermal relaxation of 71 min and 182 min, respectively (**Figure 2** and **SI**).

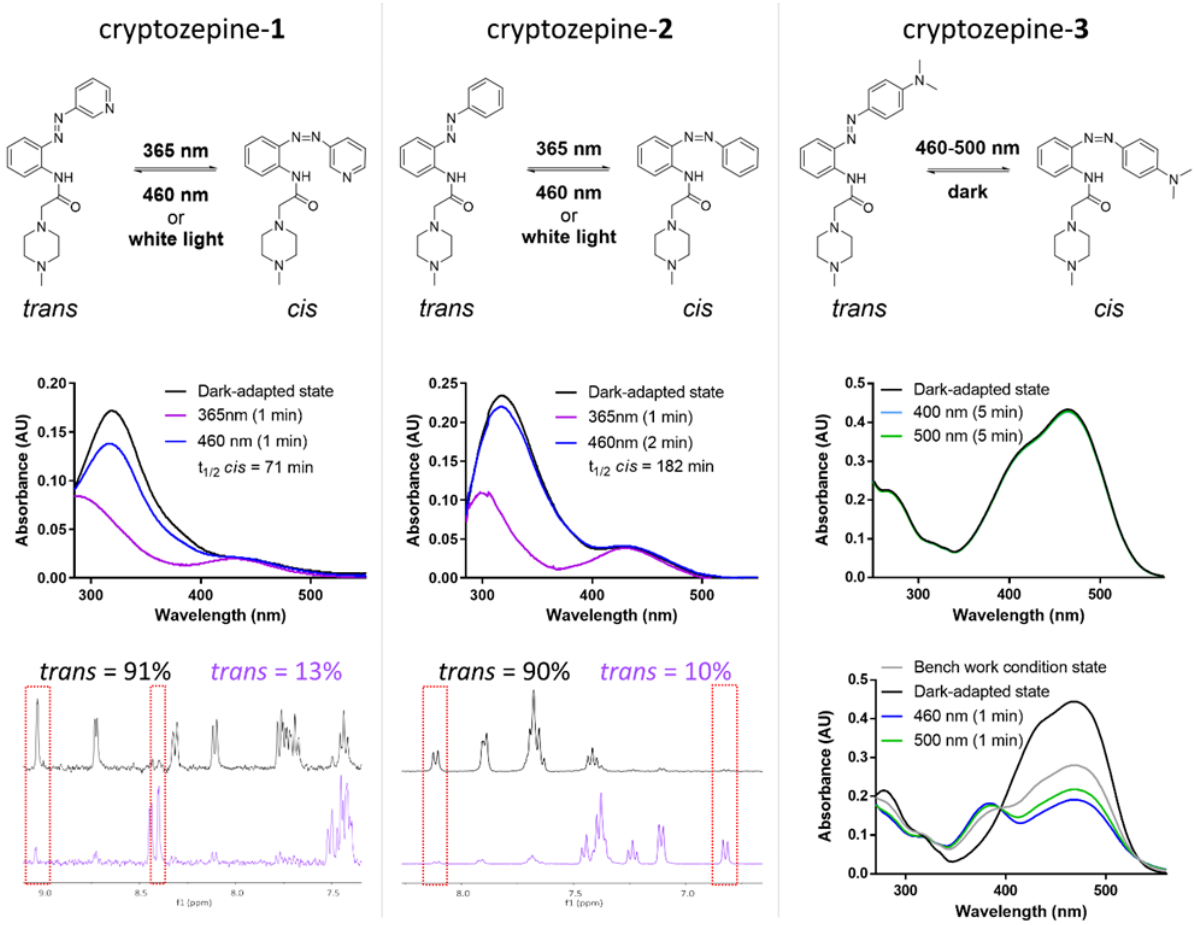

Figure 2. Photochemical characterization. Left column: absorption spectra (30 µM in H_2O) and quantification of cryptozepine-**1** photostationary state (PSS) by ^{1}H-NMR analysis (1 mM in D_2O), showing the ratio between the two isomers in the dark-adapted state (*trans* = 91%) and after illumination with 365 nm light for 5 min (*trans* = 13%). Middle column: absorption spectra (30 µM in H_2O) and quantification of cryptozepine-**2** PSS by ^{1}H-NMR analysis (1 mM in D_2O), showing the ratio between the two isomers in the dark-adapted state (*trans* = 90%) and after illumination with 365 nm light for 5 min (*trans* = 10%). Right column: absorption spectra in water (30 µM, spectra above) and absorption spectra in anhydrous DMSO (30 µM, spectra below) of cryptozepine-**3**. The switching of the red-shifted compound cryptozepine-**3** can be observed by UV-vis spectrophotometer analysis only in anhydrous solvent.

Competition Binding and Calcium Imaging Experiments at Muscarinic Receptors. We determined the affinity of pirenzepine and cryptozepines for the mAChRs by radioligand competition binding assays. For this purpose, we used Wistar rat brain membranes (whole cortex), that contain a high density of mAChRs,[28] and the non-selective muscarinic orthosteric antagonist [^{3}H]quinuclidinyl benzilate ([^{3}H]QNB) as competitive radioligand (see **SI**).[28–31] In this assay, pirenzepine has a good binding affinity in the nanomolar range, with an IC_{50} of about 50 nM (**Table 1**, and **SI**, Figure **S5.1**), and all cryptozepines showed moderate binding affinity in the low micromolar range, with cryptozepine-**2** emerging as the best ligand with an IC_{50} of about 9 μM (**Table 1**, and **SI**, Figure **S5.1**). No significant differences in affinity were observed between the *trans*- and the *cis*-enriched forms (named "*trans*" and "*cis*" from now on for the sake of simplicity) for the three cryptozepines in these experimental conditions. However, the fact that the compounds maintain the muscarinic binding despite the cleavage of the original tricyclic core encouraged us to further investigate their photopharmacological behavior through activity assays where differences between the *trans* and *cis* forms might be detected.

Ligand	Ki (M)	IC_{50} (M)
Pirenzepine	8.4 (± 1.4) x 10^{-9}	5.0 x 10^{-8}
Cryptozepine-1 (*trans*)	6.4 (± 1.4) x 10^{-6}	3.8 x 10^{-5}
Cryptozepine-1 (*cis*)	7.0 (± 2.2) x 10^{-6}	4.2 x 10^{-5}
Cryptozepine-2 (*trans*)	1.7 (± 0.3) x 10^{-6}	9.9 x 10^{-6}
Cryptozepine-2 (*cis*)	1.5 (± 0.5) x 10^{-6}	9.2 x 10^{-6}
Cryptozepine-3 (*trans*)	5.3 (± 0.1) x 10^{-6}	3.3 x 10^{-5}
Cryptozepine-3 (*cis*)	5.3 (± 0.1) x 10^{-6}	3.2 x 10^{-5}

Table 1. Muscarinic radioligand competition binding assays in Wistar rat brain membranes. The parameters shown in the table were calculated using the "Binding – Competitive – one site - Fit Ki" for Ki values, and "Binding – Competitive – one site - Fit logIC50" for the IC_{50}, which are functions in GraphPad Prism 6. Values are means ± SEM.

In particular, our data suggested to retain cryptozepine-**2** (best binding affinity) and cryptozepine-**3** (best photochromic behavior) for further studies. We performed real-time calcium imaging experiments in transiently transfected HEK cells expressing M_1 mAChR to study the antagonist behavior of our compounds (**Figure 3**). The calcium indicator OGB-1 AM (excitation at 494 nm and emission at 523 nm) was suitable for cryptozepine-**2**, while R-GECO1 (excitation at 561 nm and emission at 589 nm) was used for cryptozepine-**3** to avoid artifacts due to unwanted emission of fluorescence from OGB-1 AM upon illumination at 460 nm. The natural orthosteric agonist acetylcholine (ACh, 0.5 µM) was applied or co-applied to induce receptor activation. ACh alone induced reproducible cytosolic calcium oscillations, indicative of M_1 agonism. Both cryptozepines-**2** and **3** at 100 µM showed antagonistic behavior. Importantly, a complete recovery of ACh-induced activity was observed after the complete wash-out of the two antagonists. At 100 µM Cryptozepine-**2** reduced the total cell response by 64 (mean) (± 2.1; standard error of the mean [SEM]) % in *trans* and by 73 (± 1.6) % in *cis*. Cryptozepine-**3** did not antagonize the ACh-induced response at 100 µM in *trans*, and it reduced the cell response by 14 (± 2.6) % under continuous illumination (*cis*-enriched form) with blue light (460 nm) (**Figure 3**). Both the antagonist activity and the significant differences observed between the *trans* and *cis* states for both compounds are in agreement with the design, where a higher inhibitory activity was intended upon illumination. The stronger inhibition displayed by cryptozepine-**2** compared to cryptozepine-**3** at 100 µM is probably due to the three-fold tighter binding of the former (see **SI**, **Figure S5.1**). The activity of *trans*-cryptozepine-**2** can also be attributed to its proximity to saturation at this concentration, and could be reduced at lower concentrations. Correspondingly, cryptozepine-**3** is inactive in the dark and a (weak) inhibitor under illumination with blue light at the same concentration. We hypothesized that the electronic and/or steric properties of the additional group ($–NMe_2$) on the terminal aromatic ring in cryptozepine-**3** might account for its reduction of efficacy in comparison with cryptozepine-**2**. However, the efficiency of cryptozepine-**3** may be also limited by the relatively smaller population of *cis* isomer

that is achieved upon irradiation as a consequence of its faster relaxation. Before using our most potent antagonist, cryptozepine-**2,** for physiologically more complex experiments, we studied whether it also retained the M_1 *vs* M_2 subtype selectivity of pirenzepine. Firstly, we measured calcium responses in HEK cells expressing M_2 mAChR and observed that the antagonist behavior of cryptozepine-**2** was only partial (100 µM) or undetectable (10 µM) for this receptor subtype (**Figure 3D**). We also tested the M_1/M_2 specific affinity of the more active *cis*-cryptozepine-**2** in radioligand competition binding studies. These results also confirmed the M_1 selectivity in the µM range of concentrations (1, 10, and 100 µM), with a quite negligible M_2 affinity at 1 and 10 µM (**Figure 3E**) and estimated IC_{50} values of 1.9 µM for M_1 and 28 µM for M_2 (**Figure S5.2**). These data all together demonstrate that the crypto-azologization design yields *cis*-active light-sensitive derivatives that, not only retain the original activity of the parent compound, but also its selectivity.

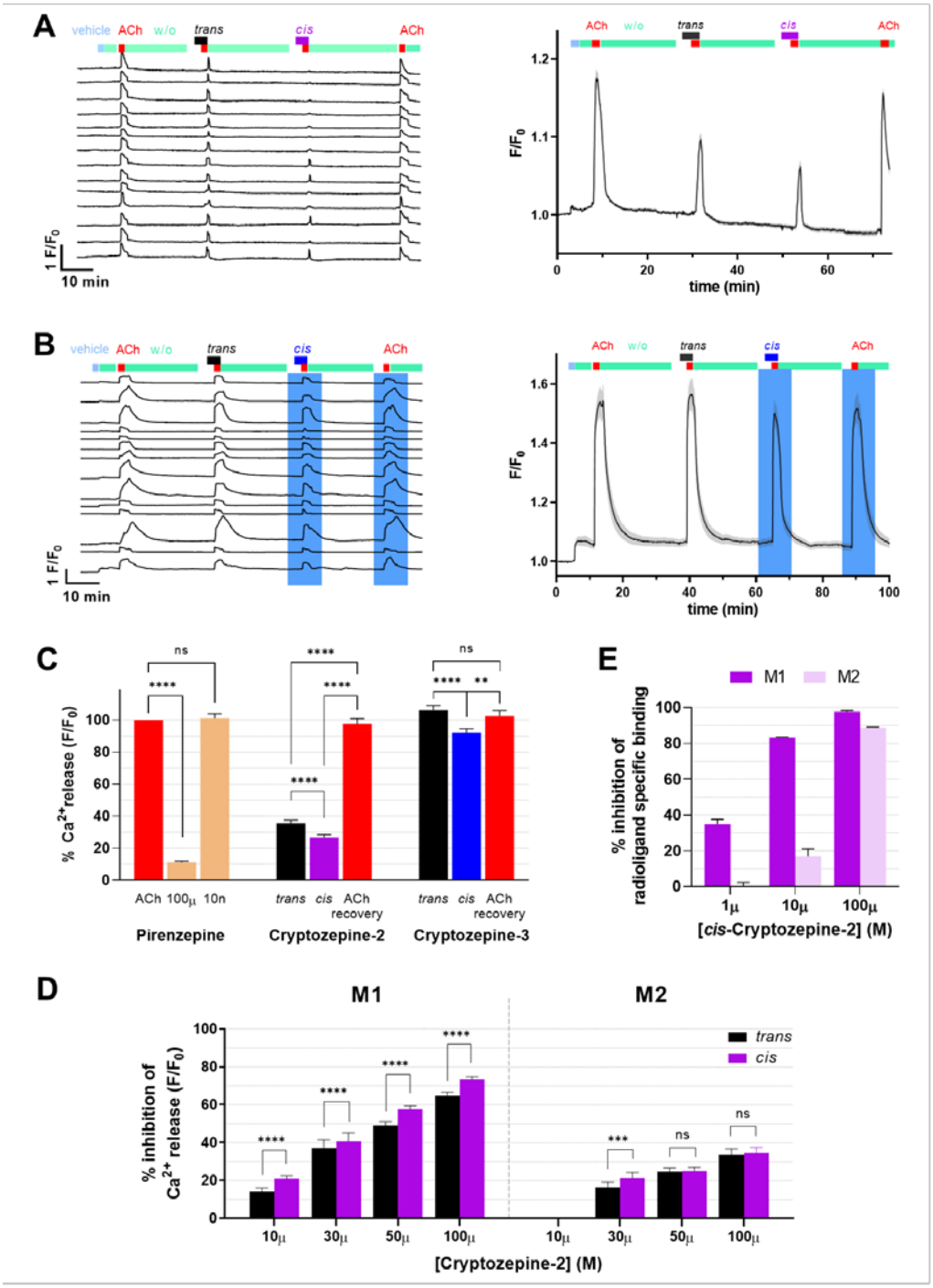

Figure 3. Cryptozepine-2 and -3 antagonism on M_1 mAChRs and cryptozepine-2 subtype-selectivity. (**A**) Cryptozepine-**2** and (**B**) Cryptozepine-**3** real-time calcium imaging response from HEK cells expressing M_1 mAChRs, loaded with 10 µM calcium indicator OGB-1 AM (representative single traces, n=14 cells, on the left; average, n = 67 cells, on the right), and co-expressing R-GECO1 as calcium indicator (representative single traces, n=14 cells, on the left; average, n = 48 cells, on the right), respectively. After 365 nm illumination, 100 µM cryptozepine-2 reduced 0.5 µM ACh responses stronger than before UV light application. Under 460 nm illumination, 100 µM cryptozepine-**3** reduced 0.5 µM

ACh responses. Grey band indicates the standard error of the mean (SEM). (**C**) Quantification of the calcium imaging responses. ACh-induced calcium release was significantly reduced by 100 μM pirenzepine and cryptozepine-**2**. *Cis*-cryptozepine-**2** shows a significant stronger inhibition than its *trans* isomer. 100 μM cryptozepine-**3** partially and significantly reduced ACh-induced calcium release only under 460 nm illumination (*cis*). Data were analyzed by paired sample Wilcoxon signed rank test (p-value (**) < 0.01, (***) < 0.001 (****) < 0.0001; GraphPad Prism 6. Error bars are ± SEM. (**D**) Calcium imaging studies of M_1 vs M_2-GqTOP selectivity with 10 (M_1, n = 183; M_2, n = 99), 30 (M_1, n = 58; M_2, n = 106), 50 (M_1, n = 262; M_2, n = 191) and 100 (M_1, n = 194; M_2, n = 165) μM cryptozepine-**2**. On M_1-expressing cells, cryptozepine-**2** significantly showed its stronger and photoswitchable antagonism than on M_2 cells. The data were normalized over the maximum response obtained with 0.5 μM ACh and analyzed by the paired sample Wilcoxon signed rank test (p-value (***) < 0.001 (****) < 0.0001; GraphPad Prism 6. Error bars are ± SEM. (**E**) Selective M_1 vs M_2 mAChRs radioligand binding inhibition of the more active *cis*-cryptozepine-**2** isomers.

Anticholinergic Effects in Mouse Isolated Atrium. To validate crypto-azologs in a physiologically relevant scenario (i.e. in tissue expressing a diversity of endogenous receptors) we tested the effect of cryptozepine-**2** on the mouse isolated atrium. Here, the excitation of muscarinic receptors induces arrest of the heartbeat.[32–34] This negative chronotropic effect in the atria is primarily mediated by mAChRs activation, including M1, and the anticholinergic activity of pirenzepine resumes the heart rate and rhythm.[32–35] We isolated the right atria from male mice and measured their spontaneous frequency of contraction (control), which was about 360 beats/min (see **SI**). Application of the muscarinic agonist carbachol (CCh, 1 μM) strongly reduces the frequency to around 200 beats/min (**Figure 4**) and addition of pirenzepine (PNZ, 1 μM) to the bath restores the frequency almost to control values (**Figure 4**). We used this robust assay to test the antagonist behavior of cryptozepine-**2** isomers. At the concentration of 100 μM, the *trans* isomer was unable to antagonize CCh-induced bradycardia and was seemingly inert, whereas *cis*-cryptozepine-**2** readily induced the partial recovery of atrium contraction frequency (**Figure 4** and **SI**). This effect is in accord with the M_1 anticholinergic activity of pirenzepine in the atria[32–35] and, considering the partial M_1 *vs* M_2 selectivity of our ligand

at 100 µM (**Figure 3**), can be attributed mainly to M_1, further highlighting the pharmacological potential of the cryptoazologization design.

Regarding future applications, the photopharmacological properties of cryptozepines should be enhanced by improving the potency of the active forms and avoiding the need of ultraviolet light, which is not optimal for biological applications. Although it is remarkable that cryptoazologs retain the activity and selectivity of the parent tricyclic compound, the actual potency achieved in our pilot study is almost 200-fold lower (see Table **1**) which prompts subsequent rounds of lead optimization and safety testing as usually carried out in drug development processes. An option for improving the optical and pharmacological properties at once might be inserting fluorine in the ortho position(s) of the azobenzene. These modifications should preserve or even improve the antagonist potency by adding lipophilic contacts in the binding pocket[16] while providing favorable photochromic properties like slow thermal back-isomerization and high two-photon cross section.[36] Furthermore, substitutions of the piperazine tail allow tuning subtype selectivity (e.g. diethyl[(piperidin-2-yl)methyl]amine yields nanomolar, M2 selective antagonists.[37,38]

Overall, the photopharmacological properties of cryptozepines set the stage for interesting assays *in vivo.* If they can be enterically administered in the inactive form (*trans*), these drugs could be remotely photoactivated at the desired location and time using the built-in LED of an endoscopy capsule,[39] potentially allowing to treat gastrointestinal tract diseases without producing (adverse) effects in other regions or organs. More invasive applications include the manipulation of cardiac function *in vivo* using optoelectronic devices coupled to cardiac patches.[14,40] In any case, to test the feasibility of future therapies based on photoswitchable drugs, both isomers must be pharmacologically characterized.

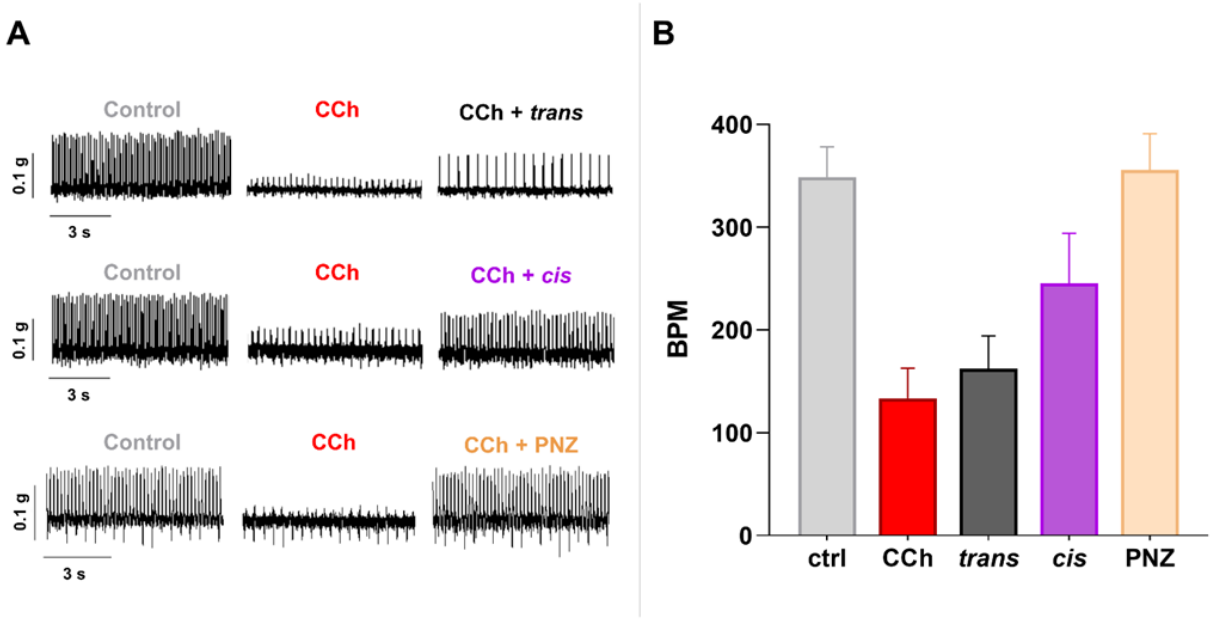

Figure 4. Pirenzepine and cryptozepine-2 can antagonize CCh-induced bradycardia in mouse atria through M1 receptors. Representative traces (Panel **A**) and quantification (Panel **B**) of mouse right atrium heart rate treated with Carbachol (CCh), pirenzepine (PNZ) and *trans*/*cis* cryptozepine-**2**. Spontaneous mechanical contractions of the mouse atria were recorded as control (ctrl) and defined as heartbeat frequency in beats/min (BPM). CCh 1 µM decreased both the amplitude and BPM. The presence of PNZ (n = 6) and *cis*-cyptozepine-*2* (*cis*) (n = 2) reversed the CCh-induced bradycardia. In contrast, *trans*-cryptozepine-**2** (*trans*) (n=2) did not reverse effect of CCh in terms of heartbeat frequency (n = 2).

CONCLUSION

In summary, we have expanded the rational design of photochromic ligands to the important class of tricyclic drugs. The proposed strategy involves two concomitant structural modifications to afford azobenzene derivatives that can mimic the tricyclic motif: (1) an isosteric replacement with a -N=N- group, and (2) a ring cleavage. We have demonstrated a proof of concept with a set of photoswitchable derivatives of the muscarinic antagonist pirenzepine that we named cryptozepines. These novel compounds retain micromolar binding and antagonist character despite the structural dissimilarity with the parent compound. The most potent photoswitchable compound (cryptozepine-**2**) displays

negligible activity in mouse atrium in *trans* and M1 antagonism in *cis*, indicating that the crypto-azologization strategy has the potential to produce photoswitchable derivatives of tricyclic drugs that are inactive in their thermally stable *trans* isomer, which is desirable in photopharmacology. Further optimization of the photochromism and of the potency of the active form might yield photopharmacological drug candidates displaying high safety and localized therapeutic action. Interestingly, cryptozepine-**2** already maintains a moderate selectivity for M1 over M2 receptors, similarly to its parent compound. The proof of concept demonstrated with this strategy opens the way to use it in many other targets bearing the tricyclic motif. This work provides a new toolbox to design photochromic drugs that significantly expands the scope of photopharmacology and its applications.

EXPERIMENTAL SECTION

Chemical synthesis

Materials and methods. All reagents and solvents were purchased from Sigma-Aldrich, Cymit Química and Serviquimia and were used without any further purification. TLC analyses were performed on commercial silica gel 60 F_{254} aluminium foils (Merck); spots were further evidenced by spraying with a dilute alkaline potassium permanganate solution or a phosphomolybdic acid solution 5% in ethanol and, for tertiary amines and quaternary ammonium compounds, with the Dragendorff reagent. Flash chromatography was performed on PanReac AppliChem silica gel 60 (40-63 microns), Biotage® SNAP KP-C18-HS 12g or Biotage® SNAP KP-SIL 25g as stationary phases; mobile phases are specified for each compound. UV-Vis spectra and experiments were recorded with a Shimadzu UV-1800 UV-VIS Spectrophotometer with standard quartz cuvettes (10 mm light path). ^{1}H-NMR and ^{13}C-NMR spectra were registered with a Varian Mercury 400 MHz (400 MHz for ^{1}H-

NMR and 101 MHz for ^{13}C-NMR) and a Varian VNMRS500 MHz instrument (500 MHz for ^{1}H-NMR and 126 MHz for ^{13}C-NMR) in DMSO-*d*$_6$, $CDCl_3$, D_2O. Residual signals of the deuterated solvents were used as an internal standard (DMSO-*d*6: ^{1}H 2.50 *ppm*, ^{13}C 39.52 *ppm*; $CDCl_3$: ^{1}H 7.26 *ppm*, ^{13}C 77.16 *ppm*; D_2O: ^{1}H 4.79 *ppm*). Chemical shifts (δ) are expressed as parts-per-million (*ppm*) and coupling constants (*J*) as hertz (*Hz*). HPLC analyses were performed with a Waters Alliance 2795 separation module (RP column: XSelect CSH C18, 50x4.6 mm, S-3.5 µm, 1.6 ml/min; eluent: from 5% B to 100% B in 3.5 min using a linear gradient, A: H_2O 0.1% formic acid, B: acetonitrile 0.1% formic acid) coupled to a Waters 2996 photodiode detector and a Waters 3100 mass spectrometer. High resolution mass spectroscopy measurements (ionization: NanoESI, positive ionization) were performed at the mass spectrometry core facility of the IRB (Barcelona, Spain) with a LTQ-FT Ultra (Thermo Scientific) for direct infusion (Automated Nanoelectrospray) of the sample. The NanoMate (AdvionBioSciences, Ithaca, NY, USA) aspirated the samples from a 384-well plate (protein Lobind) with disposable, conductive pipette tips, and infused the samples through the nanoESI Chip (which consists of 400 nozzles in a 20x20 array) towards the mass spectrometer. Spray voltage was 1.70 kV and delivery pressure was 0.50 psi. Data are reported as mass-to-charge ratio (*m/z*) of the corresponding positively charged molecular ions.

Abbreviations. Solvents: EtOAc: ethyl acetate; CH_2Cl_2: dichloromethane; MeCN: acetonitrile; MeOH: methanol; EtOH: ethanol; THF: tetrahydrofuran; Et_2O: diethyl ether; DMSO: dimethylsulfoxide. **Analytical characterizations:** NMR: d: doublet; dd: double doublet; ddd: double double doublet; dddd: doublet of doublet of doublet of doublets; dt: double triplet; m: multiplet; q: quartet; quin: quintet; s: singlet; t: triplet; m.p.: melting point; R_f: retention factor; r.t.: room temperature; RT: retention time.

Detailed characterization data are disclosed in the **Supporting Information (SI).**

***N*-(2-aminophenyl)-2-chloroacetamide (5).** Fe (1.30 g, 23.30 mmol), NH_4Cl (124.63 mg, 2.33 mmol) and glacial acetic acid (0.270 mL, 4.66 mmol) were added into 10 mL H_2O and stirred at 50 °C for 15 min. A solution of 2-chloro-N-(2-nitrophenyl)acetamide (0.5 g, 2.33 mmol) in DMF (5 mL) was added into the above solution quickly, and stirring was continued at 50 °C for 15 min. Then the reaction solution was alkalized to pH 9 with aqueous Na_2CO_3. Subsequently the mixture was filtered, and the cake was washed with H_2O and EtOAc. The combined filtrate was extracted with EtOAc. Then the combined organic layers were washed with brine, dried over anhydrous $MgSO_4$, filtered, concentrated under reduced pressure. Purification of the crude product by chromatography on silica gel (cyclohexane/EtOAc, 4:6) afforded *N*-(2-aminophenyl)-2-chloroacetamide (**5**) as a white solid (260 mg, 60%). ^{1}H NMR (400 MHz, $CDCl_3$) δ 8.19 (s, 1H), 7.31 (dd, *J* = 7.8, 1.5 Hz, 1H), 7.10 (td, *J* = 7.7, 1.5 Hz, 1H), 6.87 – 6.80 (m, 2H), 4.24 (s, 2H), 3.77 (s, 2H).

2-Chloro-*N*-(2-nitrosophenyl)acetamide (6). *N*-(2-aminophenyl)-2-chloroacetamide (**5**) (250 mg, 1.35 mmol) was suspended in 5 mL of CH_2Cl_2. Oxone® (630 mg, 2.05 mmol) in 20 mL of water was added and the resulting mixture was stirred vigorously for 1 h at room temperature. The organic phase was separated, and the aqueous phase was extracted with 10 mL of CH_2Cl_2. The combined organic phases were washed with 1 M HCl (50 mL), saturated aqueous $NaHCO_3$ (50 mL), and water (50 mL). Finally, it was dried over $MgSO_4$, and evaporated under reduced pressure to afford the nitroso derivative (**5**) which was used in the next step without further purification.

2-Chloro-N-(2-(pyridin-3-yldiazenyl)phenyl)acetamide (7a). Compound **6** (155 mg, 0.78 mmol) and 3-aminopyridine (147 mg, 1.56 mmol) were dissolved in glacial acetic acid (30 mL) and stirred for 24 h at 60 °C. The solution was diluted with water and extracted with EtOAc. The organic phase was washed four times with water and once with brine and dried over $MgSO_4$. The crude product was purified by chromatography (eluent: cyclohexane/EtOAc, 9:1) to yield **7a** (100 mg, 47%) as an orange solid. ^{1}H NMR (400 MHz, $CDCl_3$) δ 10.96 (s, 1H), 9.23 (dd, *J* = 2.4, 0.8 Hz, 1H), 8.73 (dd, *J* = 4.7,

1.6 Hz, 1H), 8.68 (dd, *J* = 8.4, 1.3 Hz, 1H), 8.15 (ddd, *J* = 8.2, 2.4, 1.6 Hz, 1H), 7.92 (dd, *J* = 8.1, 1.6 Hz, 1H), 7.55 (ddd, *J* = 8.7, 7.2, 1.6 Hz, 1H), 7.48 (ddd, *J* = 8.2, 4.8, 0.8 Hz, 1H), 7.29 – 7.22 (m, 1H), 4.29 (s, 2H). ^{13}C NMR (101 MHz, $CDCl_3$) δ 164.33, 152.27, 147.88, 147.31, 139.79, 135.65, 133.91, 127.05, 124.63, 124.31, 120.30, 120.05, 43.58.

2-Chloro-*N*-(2-(phenyldiazenyl)phenyl)acetamide (7b). Compound **6** (170 mg, 0.86 mmol) and aniline (159 mg, 1.71 mmol) were dissolved in glacial acetic acid (30 mL) and stirred for 4 days at room temperature. The solution was diluted with water and extracted with EtOAc. The organic phase was washed four times with water and once with brine and dried over $MgSO_4$. The crude product was purified by chromatography (eluent: cyclohexane/EtOAc, 9:1) to yield **7b** (130 mg, 56%) as an orange solid. ^{1}H NMR (400 MHz, $CDCl_3$) δ 11.03 (s, 1H), 8.66 (dd, *J* = 8.3, 1.3 Hz, 1H), 7.97 – 7.91 (m, 2H), 7.89 (ddd, *J* = 8.2, 1.6, 0.5 Hz, 1H), 7.56 – 7.46 (m, 4H), 7.22 (ddd, *J* = 8.2, 7.3, 1.3 Hz, 1H), 4.27 (s, 2H). ^{13}C NMR (101 MHz, $CDCl_3$) δ 164.28, 152.51, 139.63, 135.29, 132.90, 131.66, 129.39, 124.46, 123.01, 120.08, 119.98, 43.52.

2-Chloro-*N*-(2-((4-(dimethylamino)phenyl)diazenyl)phenyl)acetamide (7c). Compound **6** (500 mg, 2.52 mmol) and 4-amino-*N*,*N*-dimethylaniline (514 mg, 3.78 mmol) were dissolved in glacial acetic acid (20 mL) and stirred for 30 minutes at room temperature. The solution was concentrated under reduced pressure and the crude product was purified by chromatography (eluent: cyclohexane/AcOEt, 8:2) to afford **7c** as a red solid in quantitative yield. ^{1}H NMR (400 MHz, $CDCl_3$) δ 11.00 (s, 1H), 8.59 (dd, *J* = 8.3, 1.4 Hz, 1H), 7.94 – 7.87 (m, 2H), 7.83 (ddd, *J* = 8.1, 1.6, 0.5 Hz, 1H), 7.39 (dddd, *J* = 8.3, 7.3, 1.6, 0.5 Hz, 1H), 7.19 (dddd, *J* = 8.0, 7.3, 1.3, 0.5 Hz, 1H), 6.81 – 6.72 (m, 2H), 4.27 (s, 2H), 3.11 (s, 6H). ^{13}C NMR (101 MHz, $CDCl_3$) δ 164.04, 152.87, 143.71, 140.36, 134.62, 130.79, 125.35, 124.46, 119.78, 118.42, 111.73, 43.61, 40.43.

(*E*)-2-(4-Methylpiperazin-1-yl)-*N*-(2-(pyridin-3-yldiazenyl)phenyl)acetamide

(Cryptozepine-1). Compound **7a** (100 mg, 0.364 mmol) was dissolved in 20 mL of MeCN. 1-Methylpiperazine (55 mg, 0.547 mmol) and triethylamine (55.3 mg, 0.546 mmol) were then slowly added to the solution. The mixture was stirred under reflux for 3 h. Upon completion, MeCN was removed under reduced pressure and the obtained oil was dissolved in EtOAc. The resulting organic solution was washed 4 times using 30 mL of saturated aqueous $NaHCO_3$. The organic layer was dried over $MgSO_4$ and evaporated under reduced pressure to afford the final product (**1**) as a yellow solid (quantitative yield). ^{1}H NMR (400 MHz, $CDCl_3$) δ 10.97 (s, 1H), 9.25 (dd, *J* = 2.4, 0.8 Hz, 1H), 8.78 (dd, *J* = 8.4, 1.3 Hz, 1H), 8.74 (dd, *J* = 4.8, 1.6 Hz, 1H), 8.26 (ddd, *J* = 8.2, 2.4, 1.6 Hz, 1H), 7.81 (dd, *J* = 8.2, 1.5 Hz, 1H), 7.58 – 7.44 (m, 2H), 7.15 (ddd, *J* = 8.4, 7.3, 1.3 Hz, 1H), 3.25 (s, 2H), 2.73 – 2.39 (m, 8H), 2.23 (s, 3H). ^{13}C NMR (101 MHz, $CDCl_3$) δ 168.84, 151.95, 146.57, 139.99, 137.85, 134.10, 129.63, 128.23, 124.11, 123.65, 120.35, 116.24, 63.03, 55.04, 53.71, 45.95.

(*E*)-1-Methyl-4-(2-oxo-2-((2-(pyridin-3-yldiazenyl)phenyl)amino)ethyl)piperazine-1,4-diium chloride (Cryptozepine-1 dihydrochloride). 5 mL of 4 M HCl in dioxane were added slowly to compound **1** (10 mg, 0.03 mmol) at 0 °C. The mixture was stirred for 30 min at room temperature, then the solvent and excess of HCl were evaporated under reduced pressure and the resulting solid was washed 3 times with Et_2O (30 mL). The so obtained orange solid was dried under vacuum to afford cryptozepine-**1** dihydrochloride (quantitative yield). ^{1}H NMR (500 MHz, D_2O) δ 9.23 (s, 1H), 8.88 (s, 1H), 8.70 (d, *J* = 8.4, 1.7 Hz, 1H), 8.09 (dd, *J* = 8.3, 5.4 Hz, 1H), 8.03 (d, *J* = 8.2 Hz, 1H), 7.82 (d, *J* = 8.2, 1.5 Hz, 1H), 7.72 (t, 1H), 7.44 (t, 1H), 3.61 (s, 2H), 3.58 – 3.00 (m, 8H), 2.88 (s, 3H). ^{13}C NMR (126 MHz, D_2O) δ 170.19, 149.25, 145.58, 143.06, 140.05, 135.59, 134.71, 134.43, 127.04, 126.49, 124.01, 116.79, 59.48, 52.94, 49.49, 42.71. HR-MS (ESI, $[M + H]^+$): calcd for $C_{18}H_{23}N_6O^+$, 339.19; found 339.1930.

(*E*)-2-(4-Methylpiperazin-1-yl)-*N*-(2-(phenyldiazenyl)phenyl)acetamide (Cryptozepine-2). Compound **7b** (100 mg, 0.364 mmol) was dissolved in 20 mL of MeCN. 1-Methylpiperazine (55 mg, 0.547 mmol) and triethylamine (55.3 mg, 0.546 mmol) were then slowly added to the solution. The

mixture was stirred under reflux for 3 h. Upon completion, MeCN was removed under reduced pressure and the obtained oil was dissolved in EtOAc. The resulting organic solution was washed 4 times using 30 mL of saturated aqueous $NaHCO_3$. The organic layer was dried over $MgSO_4$ and evaporated under reduced pressure to afford the final product (**2**) as a yellow solid (quantitative yield). ^{1}H NMR (400 MHz, $CDCl_3$) δ 10.94 (s, 1H), 8.77 (dd, *J* = 8.4, 1.3 Hz, 1H), 8.07 – 7.97 (m, 2H), 7.78 (dd, *J* = 8.2, 1.6 Hz, 1H), 7.58 – 7.44 (m, 4H), 7.12 (ddd, *J* = 8.3, 7.2, 1.3 Hz, 1H), 3.23 (s, 2H), 2.82 – 2.30 (m, 8H), 2.22 (s, 3H). ^{13}C NMR (101 MHz, $CDCl_3$) δ 168.74, 152.75, 139.91, 137.41, 133.04, 131.31, 129.29, 123.49, 123.29, 120.09, 116.01, 63.02, 54.92, 53.73, 45.95.

(*E*)-1-Methyl-4-(2-oxo-2-((2-(phenyldiazenyl)phenyl)amino)ethyl)piperazine-1,4-diium chloride (Cryptozepine-2 dihydrochloride). 6 mL of 4 M HCl in dioxane were added slowly to compound **2** (50 mg, 0.15 mmol) at 0 °C. The mixture was stirred for 30 min at room temperature, then the solvent and excess of HCl were evaporated under reduced pressure and the resulting solid was washed 3 times with Et_2O (30 mL). The so obtained orange solid was dried under vacuum to afford cryptozepine-**2** dihydrochloride (quantitative yield). ^{1}H NMR (400 MHz, DMSO-d_6) δ 10.74 (s, 1H), 8.41 (d, *J* = 8.3 Hz, 1H), 8.06 – 7.91 (m, 2H), 7.84 – 7.55 (m, 5H), 7.32 – 7.25 (m, 1H), 3.52 – 2.87 (m, 10H), 2.69 (s, 3H). ^{13}C NMR (126 MHz, DMSO-d_6) δ 153.28, 152.26, 136.30, 132.77, 131.81, 129.58, 128.87, 124.48, 122.98, 120.02, 116.13, 58.52, 50.68, 48.77, 41.88. HR-MS (ESI, $[M + H]^+$): calcd for $C_{19}H_{24}N_5O^+$, 338.20; found 338.1968.

(*E*)-N-(2-((4-(Dimethylamino)phenyl)diazenyl)phenyl)-2-(4-methylpiperazin-1-yl)acetamide (Cryptozepine-3). Compound **7c** (20 mg, 0.063 mmol) was dissolved in 20 mL of MeCN. 1-Methylpiperazine (9.5 mg, 0.095 mmol) and triethylamine (9.58 mg, 0.095 mmol) were then slowly added to the solution. The mixture was stirred under reflux for 3 h. Upon completion, MeCN was removed under reduced pressure and the obtained oil was dissolved in EtOAc. The resulting organic solution was washed 4 times using 30 mL of saturated aqueous $NaHCO_3$. The organic layer was dried over $MgSO_4$ and evaporated under reduced pressure to afford the final product (**3**) as a yellow solid

(quantitative yield). ^{1}H NMR (400 MHz, $CDCl_3$) δ 10.90 (s, 1H), 8.72 (dd, *J* = 8.4, 1.3 Hz, 1H), 8.03 – 7.98 (m, 2H), 7.75 (dd, *J* = 8.1, 1.6 Hz, 1H), 7.38 (ddd, *J* = 8.6, 7.3, 1.6 Hz, 1H), 7.11 (ddd, *J* = 8.3, 7.3, 1.4 Hz, 1H), 6.82 – 6.74 (m, 2H), 3.24 (s, 2H), 3.11 (s, 6H), 2.83 – 2.43 (m, 8H), 2.29 (s, 3H). ^{13}C NMR (101 MHz, $CDCl_3$) δ 168.61, 152.65, 143.93, 140.49, 136.28, 131.02, 125.61, 123.56, 119.80, 115.65, 111.67, 63.13, 54.97, 53.78, 45.98, 40.43.

(*E*)-1-(2-((2-((4-(Dimethylamino)phenyl)diazenyl)phenyl)amino)-2-oxoethyl)-4-methylpiperazine-1,4-diium (Cryptozepine-3 dihydrochloride). 6 mL of 4 M HCl in dioxane were added slowly to compound **3** (10 mg, 0.026 mmol) at 0 °C. The mixture was stirred for 30 min at room temperature, then the solvent and excess of HCl were evaporated under reduced pressure and the resulting solid was washed 3 times with Et_2O (30 mL). The so obtained orange solid was dried under vacuum to afford cryptozepine-**3** dihydrochloride (quantitative yield). ^{1}H NMR (400 MHz, D_2O) δ 8.01 (d, *J* = 8.2 Hz, 1H), 7.91 – 7.77 (m, 2H), 7.65 – 7.53 (m, 2H), 7.36 (d, 3H), 3.82 – 2.61 (m, 19H). ^{13}C NMR (101 MHz, D_2O) δ ^{13}C NMR (101 MHz, D_2O) δ 168.82, 149.08, 147.06, 141.60, 133.70, 131.88, 125.79, 125.00, 122.23, 116.67, 116.55, 59.48, 52.67, 49.44, 42.72, 42.67. HR-MS (ESI, $[M + H]^+$): calcd for $C_{21}H_{29}N_6O^+$, 381.24; found 381.2387.

2-Fluoro-4-nitro-1-nitrosobenzene (8). 2-Fluoro-4-nitroaniline (500 mg, 3.20 mmol) was suspended in 10 mL of CH_2Cl_2. Oxone® (2.46 g, 8.00 mmol) in 20 mL of water was then added and the resulting mixture was stirred vigorously for 24 h at room temperature. The organic phase was separated, and the aqueous phase was further extracted with 10 mL of CH_2Cl_2 for 3 times. The combined organic phases were washed with 1 M HCl (50 mL), saturated aqueous $NaHCO_3$ (50 mL), and water (50 mL). Finally, it was dried over $MgSO_4$, concentrated under reduced pressure, and purified by chromatography (eluent: cyclohexane/EtOAc, 9:1) to yield **8** as a green solid (300 mg, 55%) which was immediately used in the following step without further purification.

2-Chloro-*N*-(2-((2-fluoro-4-nitrophenyl)diazenyl)phenyl)acetamide (9). Compounds **5** (500 mg, 2.71 mmol) and **8** (250 mg, 1.47 mmol) were dissolved in glacial acetic acid (20 mL) and the resulting solution was stirred for 24 h at room temperature. The solution was then concentrated under reduced pressure and the crude material was purified by chromatography (eluent: cyclohexane/EtOAc, 9:1). The so obtained solid was further purified by crystallization from methanol to yield **9** as an orange solid (200 mg, 40%). ^{1}H NMR (400 MHz, $CDCl_3$) δ 10.83 (s, 1H), 8.70 (dd, J = 8.5, 1.3 Hz, 1H), 8.33 – 8.08 (m, 2H), 7.95 (dd, J = 8.2, 1.6 Hz, 1H), 7.90 – 7.84 (m, 1H), 7.61 (ddd, J = 8.7, 7.4, 1.6 Hz, 1H), 7.30 – 7.24 (m, 1H), 4.29 (s, 2H). ^{13}C NMR (101 MHz, $CDCl_3$) δ 164.35, 144.45, 140.28, 136.53, 135.36, 126.98, 124.83, 124.75, 120.49, 120.07, 119.85, 119.81, 119.23, 43.56.

(*E*)-*N*-(2-((2-Fluoro-4-nitrophenyl)diazenyl)phenyl)-2-(4-methylpiperazin-1-yl)acetamide (Cryptozepine-4). Compound **9** (200 mg, 0.594 mmol) was dissolved in 20 mL of MeCN. 1-Methylpiperazine (89.24 mg, 0.891 mmol) and triethylamine (90.16 mg, 0.891 mmol) were then slowly added to the solution. The mixture was stirred under reflux for 3 h. Upon completion, MeCN was removed under reduced pressure and the obtained oil was dissolved in EtOAc. The resulting organic solution was washed 4 times using 30 mL of saturated aqueous $NaHCO_3$. The organic layer was dried over $MgSO_4$ and evaporated under reduced pressure to afford the desired final compound (**4**) as an orange solid (quantitative yield). ^{1}H NMR (400 MHz, $CDCl_3$) δ 10.94 (s, 1H), 8.80 (dd, *J* = 8.5, 1.3 Hz, 1H), 8.27 – 8.11 (m, 2H), 8.04 – 7.93 (m, 1H), 7.85 (dd, *J* = 8.3, 1.6 Hz, 1H), 7.58 (ddd, *J* = 8.6, 7.2, 1.6 Hz, 1H), 7.16 (ddd, *J* = 8.4, 7.2, 1.3 Hz, 1H), 3.26 (s, 2H), 2.80 – 2.30 (m, 8H), 2.21 (s, 3H). ^{13}C NMR (101 MHz, $CDCl_3$) δ 168.86, 160.09, 157.48, 140.43, 138.63, 135.52, 123.79, 120.55, 119.88, 119.43, 116.84, 113.78, 113.53, 62.93, 55.17, 53.63, 46.07. HR-MS (ESI, $[M + H]^+$): calcd for $C_{19}H_{22}FN_6O_3^+$, 401.17; found 401.1732.

In vitro radioligand competition binding experiments

The affinity of our compounds and pirenzepine (PNZ) for mAChRs was studied by radioligand competition binding experiments (see **Table 1** and **Figure S5.1**). Wistar rat brain membranes (whole cortex), that contain a high density of mAChRs, were used for this assay.[28] The muscarinic antagonist [^{3}H]quinuclidinyl benzilate ([^{3}H]QNB) in ethanol solution from Amersham Biosciences (catalog number TRK 604, 42 Ci/mmol, 1 mCi/mL) was used as competitive radioligand.[30,41] Specific binding was defined with the new ligands at total nominal concentrations ranging from 1 or 10 nM to 300 µM, and derivatizing the raw disintegrations per minute (dpm) data from the scintillation counter to show the total radioactivity.[28] Binding assays were carried out as already reported by Claro, E.[28] Brain membranes were prepared from 2-3-month-old female rats. The meninges were cleaned with buffer-soaked filter paper, cortices were dissected, and white matter was trimmed off. The tissues were homogenized in 40 mL tris-HCl buffer using a Potter homogenizer with a motor-driven Teflon pestle. The homogenate was centrifuged (30 min at 50,000xg). The resulting pellet was homogenized and centrifuged again under the same conditions. Bradford assay permitted protein determination. The final pellet was resuspended at 1 mg of protein/mL, transferred to 1 mL microcentrifuge tubes, and centrifuged again. After discarding the supernatant, membrane pellets were kept at -80 °C until use. During the assay, in 5 mL tubes (24 tubes in each experiment repetition), a total volume of 2 mL of tris-HCl buffer with 6 mM $MgCl_2$ was used, containing 30 µg mAChRs proteins, 200 pM [^{3}H]QNB concentration ([^{3}H]QNB Kd = 40 pM), and the correct amount of our ligands. These conditions ensure less than 10% ligand depletion at equilibrium, which was reached with 30 min at 37 ºC incubation. Unbound ligand and radioligand were separated from the membrane samples by rapid filtration through Whatman GF/C glass microfibre filters using a manyfold Brandel device. Nonspecific binding was independent of protein concentration and defined with 2 uM atropine. It resulted to be lower than 5% of total binding.

In vitro calcium imaging experiments

Cell culture and transfection for calcium imaging. TsA201 cells were purchased from the European Collection of Authenticated Cell Culture. Cells were maintained at 37 °C in a humidified atmosphere with 5% CO_2 and grown in Dulbecco's Modified Eagle's Medium/Nutrient Mixture F-12 Ham (DMEM/F12 1:1, Life Technologies) medium, supplemented with 10% fetal bovine serum (FBS, Life Technologies) and antibiotics (1% penicillin/streptomycin, Sigma-Aldrich). The cells were transiently transfected with the human M1 receptor (Addgene), co-transfected with M1 and R-GECO1 (ratio 1:1) or human M2 receptor (Addgene) and chimeric Gi/Gq protein (GqTOP) (ratio 1:1), using X-tremeGENE 9 DNA Transfection Reagent (Roche Applied Science) following the manufacturer's instructions. As generally known, M_1 mAChRs prevalently activate Gq proteins and leads to the activation of the phospholipase C pathway, resulting in the production of inositol 1,4,5-trisphosphate (IP3) and the subsequent release of intracellular calcium from the endoplasmic reticulum. In contrast the M_2 mAChR prevalently activates the Gi protein, therefore we co-transfected the cells with a chimeric Gq/i-protein, which couples M_2 activation with the phospholipase C pathway. After 24 hours, cells were harvested with accutase (Sigma-Aldrich) and plated onto 16-mm glass coverslips (Fisher Scientific) pretreated with poly-L-Lysine (Sigma-Aldrich) to allow cell adhesion. Preconfluent cultures were used for experiments between 48 h and 72 h after transfection.

In vitro single-cell calcium imaging. The bath solution used for single cell intracellular calcium recordings contained: 140 mM NaCl, 5.4 mM KCl, 1 mM $MgCl_2$, 10 mM HEPES, 10 mM glucose and 2 mM $CaCl_2$ (pH 7.4). The calcium indicator used to test cryptozepine-**2** was OGB-1 AM (Life Technologies). Before each experiment, cells were mounted on the recording chamber (Open Diamond Bath Imaging Chamber for Round Coverslips from Warner Instruments) and loaded with OGB-1AM for 30 min at 37 °C with 5% CO_2, at a final concentration of 10 μM in Ca^{2+}-free bath solution. Cells were rinsed with fresh solution, and the recording chamber was filled with 1 mL recording solution and placed on an IX71 inverted microscope (Olympus) with a XLUMPLFLN 20XW x20/1 water immersion objective (Olympus). OGB-1 AM was excited during 50 ms at 488

nm by using a Polychrome V light source (Till Photonics) equipped with a Xenon Short Arc lamp (Ushio) and a 505-nm dichroic beam splitter (Chroma Technology). Emission at 510 nm was filtered by a D535/40 nm emission filter (Chroma Technology) and finally collected by a C9100-13 EM-CCD camera (HAMAMATSU). R-GECO1 was used as a Ca^{2+} fluorescent indicator because it absorbs less than OGB1-AM at 460 nm, wavelength used to photoisomerize the compound cryptozepine-3. R-GECO1 was excited during 50 ms at 562 nm by using a Polychrome V light source (Till Photonics) equipped with a Xenon Short Arc lamp (Ushio) and a 585-nm dichroic beam splitter (Chroma Technology). Emission at 600 nm was filtered by ET630/75nm emission filter (Chroma Technology) and finally collected by a C9100-13 EM-CCD camera (HAMAMATSU). Images were acquired at room temperature with an imaging interval of 2 sec with the SmartLux software (HEKA), and the imaging analysis was done with FIJI (ImageJ). The agonist used to stimulate M_1 and M_2 receptors in HEK tsA201 cells was acetylcholine (ACh, Sigma). Application of the compounds was carried out by manually pipetting a small volume during imaging acquisition into the accessory pool of the recording chamber for the final dilution of approximately 1:1000. Every application of 0.5 ACh μM was followed by the next application after a 20-min recovery time. The effect of these photoswitchable antagonists on the ACh-induced calcium signal was observed by applying for 2 minutes each compound (100 μM) in its *trans* or *cis* form prior to the ACh application. The subtype-selectivity study (M_1 vs M_2 mAChRs) of cryptozepine-**2** was performed by comparing the amplitude of calcium signal response of cells expressing M_2-GqTOP or M_1 mAChR in presence of different concentrations of cryptozepine-**2** (10, 30, 50 and 100 μM). Data were normalized over the maximum response obtained with ACh at 0.5 μM. In the case of pirenzepine, it was applied at decreasing concentrations ranging from 10 nM to 100 μM, 2 minutes before ACh. Photoisomerization of cryptozepine-**2** was achieved by pre-illuminating the compounds with Vilber Lourmat UV Lamp (365 nm, 6 W) for 2 min before application. Photoisomerization of cryptozepine-**3** was achieved by continuously illuminating the specimen with 460 nm light. Numerical data were imported to

GraphPad Prism version 6.00 for Windows (GraphPad Software, La Jolla, CA, USA). Statistical analysis was performed using the paired sample Wilcoxon signed rank test.

In vitro specific M1 and M2 muscarinic binding assays study of *cis*-Cryptozepine-2

The *in vitro* radioligand binding assay of 1, 10 and 100 µM *cis*-Cryptozepine-**2** enriched form (active isomer) was assessed on recombinant human M_1 and M_2 receptors expressed in Chinese hamster ovary (CHO) cells. A 10 mM DMSO stock solution of the compound was used for the assay after 30 min irradiation with 365 nm light, in order to work with a high percentage of the active cis isomer (> 80%). Compound affinity was calculated as a percentage inhibition of the binding of a radioactively labeled antagonist specific for each target in order to assess the subtype specific binding of Cryptozepine-2. In particular, 2 nM [^{3}H]-pirenzepine for M1 and 2 nM [^{3}H]AF-DX 384 for M_2 were used as subtype-selective radioligand. The evaluation of the affinity of cryptozepine-2 for the human M_1 receptor was carried out using cell membrane homogenates (45 µg protein) incubated for 60 min at 22 °C with 2 nM [^{3}H]pirenzepine (Kd = 13 nM) in the absence or presence of the test compound in a buffer containing 50 mM Tris-HCl (pH 7.4), 120 mM NaCl, 5 mM KCl, 5 mM MgCl2 and 1 mM EDTA. Nonspecific binding was determined in the presence of 1 µM atropine. Following incubation, the samples were filtered rapidly under vacuum through glass fiber filters (GF/B, Packard) presoaked with 0.3% PEI and rinsed several times with ice-cold 50 mM Tris-HCl using a 96-sample cell harvester (Unifilter, Packard). The filters are dried then counted for radioactivity in a scintillation counter (Topcount, Packard) using a scintillation cocktail (Microscint 0, Packard). The standard reference compound was pirenzepine, which was tested in each experiment at several concentrations to obtain a competition curve from which its IC_{50} is calculated.[42]

For evaluating the affinity of cryptozepine-**2** for the human M_2 receptor, cell membrane homogenates (60 µg protein) were incubated with 2 nM [3H]AF-DX 384 (Kd = 4.6 nM) following the same procedure described for the M1 receptors. The standard reference compound was methoctramine,

which was tested in each experiment at several concentrations to obtain a competition curve from which its IC_{50} is calculated.[42] Results showing an inhibition higher than 50% are considered to represent significant effects of the test compounds. Results showing an inhibition between 25% and 50% are indicative of weak to moderate effects. Results showing an inhibition lower than 25% are not considered significant. Experiments were performed in duplicate and accepted in accordance with Eurofins Cerep Quality Control Unit's validation standard operating procedure.

***Ex vivo* mice atria tissue experiments**

Animals and tissue samples. Ten CD1 male mice of 10-12 weeks old were used. Housing was under controlled conditions: constant temperature (22 ± 2ºC) and humidity (55 ± 10%), 12-hour light/dark cycle and *ad libitum* access to water and food. Before euthanasia, heparin (100 units/kg IP) was administered. Animals were sacrificed by cervical dislocation under sedation with ketamine (80 mg/kg IP) and xylazine (10 mg/kg IP). For functional studies, heart was quickly removed and placed in carbogenated (95% 0_2 and 5% $C0_2$) Krebs solution (composition in mmol/L: glucose 10.10, NaCl 115.48, $NaHCO_3$ 21.90, KCl 4.61, NaH_2PO_4 1.14, $CaCl_2$ 2.50 and $MgSO_4$ 1.16) (pH 7.4). Functional experiments were approved by the Ethics Committee of the Universitat Autònoma de Barcelona (code EUT-MJ001).

Functional studies. Right atrium was isolated and mounted in a 10-mL chamber using a compact organ bath (Panlab sl). Tissue was bathed in a carbogenated Krebs solution maintained at 37 ± 1 ºC using an external thermostat. Mechanical activity was measured with an isometric force transducer connected to a computer through an amplifier associated with PowerLab/800. LabChart software was used for data digitalization (1000 samples/s) and measurements. A tension of 0.2 g was applied, and tissue was allowed to equilibrate for 5 to 10 min, until spontaneous mechanical contractions were recorded. Carbachol 10^{-6} M was added for 3 minutes and then pirenzepine (PNZ) 10^{-6} M and 10^{-5} M, *trans*-cryptozepine-**2** (*trans*) 10^{-5} M, $3*10^{-5}$ M and 10^{-4} M or *cis*-cryptozepine-**2** (*cis*) 10^{-5} M, $3*10^{-5}$

M and 10^{-4} M were applied. Amplitude and beats per minute (beats/min, bpm) were calculated before and after the addition of the drug. Atrial contractions were recorded at a frequency of about 360 beats/min and a mean amplitude of 0.1 g. Carbachol (CCh) concentration dependently decreased both the amplitude and beats/min (n = 6) with an EC50 of about 10^{-6} M. This concentration of CCh was used to activate muscarinic receptors in the bioassay and induces bradycardia. The presence of both pirenzepine (PNZ) (n = 6) and *cis*-cryptozepine-**2** (***cis***) (n = 2) concentration-dependently reversed the effect of CCh 10^{-6} M in terms of heartbeat frequency. In contrast, *trans*-cryptozepine-**2** (***trans***) (n = 2) did not reserve CCh-induced bradycardia (n = 2) (**Figures 4**, **S7.1** and **S7.2**).

AUTHOR INFORMATION

Corresponding Author

*Corresponding author. E-mail: pau@icrea.cat

Present Addresses

†Present address Fabio Riefolo: Teamit Research, Barcelona Health Hub, Barcelona 08025, Spain.

¤Present address Simone Vitiello: Department of Life Sciences, University of Modena and Reggio Emilia, Via Campi 103, 41125 Modena, Italy.

Author Contributions

The manuscript was written through contributions of all authors.

All authors have given approval to the final version of the manuscript.

‡Rosalba Sortino and Carlo Matera contributed equally.

Funding Sources

This project has received funding from the EU Horizon 2020 Framework Programme for Research and Innovation under the Specific Grant Agreement 2 (Human Brain Project WaveScalES SGA2 No. 785907), AGAUR/Generalitat de Catalunya (CERCA Programme, 2017-SGR-1442 and 2017-SGR-1548), FEDER funds, ERANET Syn-Bio MODULIGHTOR, MINECO (FPI fellowship BES-2014−068169 and project CTQ2016−80066R), Ministerio de economia, Industria y competitividad (SAF2017-88019-C3-1-R). We also acknowledge the CECH project co-financed by the European Union Regional Development Fund within the framework of the ERDF Operational Program of Catalonia 2014-2020.

Notes

The authors declare no competing financial interest.

ACKNOWLEDGMENT

The authors are grateful to Jean-Philippe Pin for providing the chimeric Gi/Gq protein clone. Molecular graphics and analyses were performed with the UCSF Chimera package. Chimera is developed by the Resource for Biocomputing, Visualization, and Informatics at the University of California, San Francisco (supported by NIGMS P41-GM103311). Mass spectrometry was performed at the IRB Barcelona Mass Spectrometry Core Facility, which actively participates in the BMBS European COST Action BM 1403 and is a member of Proteored, PRB2- ISCIII, supported by grant PRB2 (IPT13/0001 − ISCIIISGEFI/FEDER). We thank Dr. Unai Elezcano and Dr. Sònia Varón from the Analysis and Chemistry Platform (PQA-PCB) at Barcelona Science Park for their help in HPLC-MS experiments throughout the project. All animal procedures were experiments were approved by the Ethics Committee of the Universitat Autònoma de Barcelona (code EUT-MJ001).

ASSOCIATED CONTENT

Supporting Information Availability

The Supporting Information is available free of charge on the ACS Publications website at ...

Molecular docking simulations, HPLC analyses and Mass Spectra, Photochemical characterization, NMR spectroscopy, *In vitro* radioligand competition binding experiments, *In vitro* calcium imaging experiments, *Ex vivo* mice atria tissue experiments (PDF).

Molecular formula strings (CSV)

REFERENCES

(1) Lerch, M. M.; Hansen, M. J.; van Dam, G. M.; Szymanski, W.; Feringa, B. L. Emerging Targets in Photopharmacology. *Angew. Chemie Int. Ed.* **2016**, *55*, 10978–10999.

(2) Hüll, K.; Morstein, J.; Trauner, D. In Vivo Photopharmacology. *Chemical Reviews*. American Chemical Society, **2018**, 10710–10747.

(3) Morstein, J.; Awale, M.; Reymond, J. L.; Trauner, D. Mapping the Azolog Space Enables the Optical Control of New Biological Targets. *ACS Cent. Sci.* **2019**, *5*, 607–618.

(4) Pittolo, S.; Gómez-Santacana, X.; Eckelt, K.; Rovira, X.; Dalton, J.; Goudet, C.; Pin, J. P.; Llobet, A.; Giraldo, J.; Llebaria, A.; Gorostiza, P. An Allosteric Modulator to Control Endogenous G Protein-Coupled Receptors with Light. *Nat. Chem. Biol.* **2014**, *5*, 813-815.

(5) Schoenberger, M.; Damijonaitis, A.; Zhang, Z.; Nagel, D.; Trauner, D. Development of a New Photochromic Ion Channel Blocker via Azologization of Fomocaine. *ACS Chem. Neurosci.* **2014**, *5*, 514–518.

(6) Matera, C.; Gomila, A. M. J.; Camarero, N.; Libergoli, M.; Soler, C.; Gorostiza, P. Photoswitchable Antimetabolite for Targeted Photoactivated Chemotherapy. *J. Am. Chem. Soc.* **2018**, *140*, 15764–15773.

(7) Agnetta, L.; Decker, M. Photoresponsive Hybrid Compounds. In *Design of Hybrid Molecules for Drug Development*; Elsevier Inc., 2017; 279–315.

(8) Yet, L. *Privileged Structures in Drug Discovery*; John Wiley & Sons, Inc.: Hoboken, NJ, USA, 2018.

(9) Evans, B. E.; Rittle, K. E.; Bock, M. G.; DiPardo, R. M.; Freidinger, R. M.; Whitter, W. L.; Lundell, G. F.; Veber, D. F.; Anderson, P. S.; Chang, R. S. L.; Lotti, V. J.; Cerino, D. J.; Chen, T. B.; Kling, P. J.; Kunkel, K. A.; Springer, J. P.; Hirshfield, J. Methods for Drug Discovery: Development of Potent, Selective, Orally Effective Cholecystokinin Antagoniststs. *J. Med. Chem.* **1988**, *31*, 2235–2246.

(10) Marsh, W. Tricyclic Antidepressants. In *xPharm: The Comprehensive Pharmacology Reference*; Elsevier Inc., 2007; 1–3.

(11) Fedi, V.; Guidi, A.; Altamura, M. Tricyclic Structures in Medicinal Chemistry: An Overview of Their Recent Uses in Non-CNS Pathologies. *Mini-Reviews Med. Chem.* **2008**, *8*, 1464–1484.

(12) Matera, C.; Tata, A. Pharmacological Approaches to Targeting Muscarinic Acetylcholine Receptors. *Recent Pat. CNS Drug Discov.* **2014**, *9*, 85–100.

(13) Kruse, A. C.; Kobilka, B. K.; Gautam, D.; Sexton, P. M.; Christopoulos, A.; Wess, J. Muscarinic Acetylcholine Receptors: Novel Opportunities for Drug Development. *Nature Reviews Drug Discovery*. Nature Publishing Group, **2014**, *13*, 549–560.

(14) Riefolo, F.; Matera, C.; Garrido-Charles, A.; Gomila, A. M. J.; Sortino, R.; Agnetta, L.; Claro, E.; Masgrau, R.; Holzgrabe, U.; Batlle, M.; Decker, M.; Guasch, E.; Gorostiza, P. Optical Control of Cardiac Function with a Photoswitchable Muscarinic Agonist. *J. Am. Chem. Soc.* **2019**, *141*, 7628–7636.

(15) Agnetta, L.; Kauk, M.; Canizal, M. C. A.; Messerer, R.; Holzgrabe, U.; Hoffmann, C.; Decker,

M. A Photoswitchable Dualsteric Ligand Controlling Receptor Efficacy. *Angew. Chemie Int. Ed.* **2017**, *56*, 7282–7287.

(16) Agnetta, L.; Bermudez, M.; Riefolo, F.; Matera, C.; Claro, E.; Messerer, R.; Littmann, T.; Wolber, G.; Holzgrabe, U.; Decker, M. Fluorination of Photoswitchable Muscarinic Agonists Tunes Receptor Pharmacology and Photochromic Properties. *J. Med. Chem.* **2019**, *62*, 3009–3020.

(17) Hammer, R.; Berrie, C. P.; Birdsall, N. J. M.; Burgen, A. S. V.; Hulme, E. C. Pirenzepine Distinguishes between Different Subclasses of Muscarinic Receptors [28]. *Nature*. **1980**, 283, 90–92.

(18) El-Obeild, H. A.; Babhair, S. A.; Al-Badr, A. A. Pirenzepine Dihydrochloride. *Anal. Profiles Drug Subst. Excipients* **1987**, *16*, 445–506.

(19) Eberlein, W. G.; Engel, W. W.; Trummlitz, G.; Schmidt, G.; Hammer, R. Tricyclic Compounds as Selective Antimuscarinics. 2. Structure-Activity Relationships of M1 Selective Antimuscarinics Related to Pirenzepine. *J. Med. Chem.* **1988**, *31*, 1169–1174.

(20) Encyclopedia of Psychopharmacology | Ian P. Stolerman | Springer https://www.springer.com/gp/book/9783540687061#aboutAuthors (accessed Apr 3, 2020).

(21) Walline, J. J.; Lindsley, K.; Vedula, S. S.; Cotter, S. A.; Mutti, D. O.; Twelker, J. D. Interventions to Slow Progression of Myopia in Children. *Cochrane Database Syst. Rev.* **2011**, 12. https://doi.org/10.1002/14651858.cd004916.pub3.

(22) Pedretti, R. F. E.; Prete, G.; Foreman, R. D.; Adamson, P. B.; Vanoli, E. Autonomic Modulation during Acute Myocardial Ischemia by Low-Dose Pirenzepine in Conscious Dogs with a Healed Myocardial Infarction: A Comparison with β-Adrenergic Blockade. *J.*

Cardiovasc. Pharmacol. **2003**, *41*, 671–677.

(23) Thal, D. M.; Sun, B.; Feng, D.; Nawaratne, V.; Leach, K.; Felder, C. C.; Bures, M. G.; Evans, D. A.; Weis, W. I.; Bachhawat, P.; Kobilka, T. S.; Sexton, P. M.; Kobilka, B. K.; Christopoulos, A. Crystal Structures of the M1 and M4 Muscarinic Acetylcholine Receptors. *Nature* **2016**, *531*, 335–340.

(24) Murgolo, N. J.; Kozlowski, J.; Tice, M. A. B.; Hollinger, F. P.; Brown, J. E.; Zhou, G.; Taylor, L. A.; McQuade, R. D. The N4 Nitrogen of Pirenzepine Is Responsible for Selective Binding of the M1 Subtype Human Muscarinic Receptor. *Bioorganic Med. Chem. Lett.* **1996**, *6*, 785–788.

(25) Dong, M.; Babalhavaeji, A.; Samanta, S.; Beharry, A. A.; Woolley, G. A. Red-Shifting Azobenzene Photoswitches for in Vivo Use. *Acc. Chem. Res.* **2015**, *48*, 2662–2670.

(26) Ghetti, F.; Griesbeck, A. G.; Oelgemöller, M. *CRC Handbook of Organic Photochemistry and Photobiology*; CRC Press, 2012.

(27) Bandara, H. M. D.; Burdette, S. C. Photoisomerization in Different Classes of Azobenzene. *Chemical Society Reviews*. **2012**, *41*, 1809–1825.

(28) Claro, E. Analyzing Ligand Depletion in a Saturation Equilibrium Binding Experiment. *Biochem. Mol. Biol. Educ.* **2006**, *34*, 428–431.

(29) Yamamura, H. I.; Snyder, S. H. Muscarinic Cholinergic Binding in Rat Brain. *Proc. Natl. Acad. Sci. U. S. A.* **1974**, *71*, 1725–1729.

(30) Sallés, J.; Wallace, M. A.; Fain, J. N. Differential Effects of Alkylating Agents on the Multiple Muscarinic Receptor Subtypes Linked to Activation of Phospholipase C by Carbachol in Rat Brain Cortical Membranes. *J. Pharmacol. Exp. Ther.* **1993**, *264*, 521-529.

(31) Massoulié, J.; Carson, S.; Kato, G. Biochemical Characterization of Muscarinic Receptors: Multiplicity of Binding Components. *Prog. Brain Res.* **1979**, *49*, 303–311.

(32) Heijman, J.; Kirchner, D.; Kunze, F.; Chrétien, E. M.; Michel-Reher, M. B.; Voigt, N.; Knaut, M.; Michel, M. C.; Ravens, U.; Dobrev, D. Muscarinic Type-1 Receptors Contribute to IK,ACh in Human Atrial Cardiomyocytes and Are Upregulated in Patients with Chronic Atrial Fibrillation. *Int. J. Cardiol.* **2018**, *255*, 61–68.

(33) Süsskand, K.; Sewing, K.-F. Anticholinergic Effects of Pirenzepine on the Guinea-Pig Isolated Atrium. *Pharmacology* **1979**, *19*, 163–164.

(34) Woo, S. H.; Byung, H. L.; Kwon, K. Il; Chin, O. L. Excitatory Effect of M1 Muscarinic Acetylcholine Receptor on Automaticity of Mouse Heart. *Arch. Pharm. Res.* **2005**, *28*, 930–935.

(35) Hogan, K.; Markos, F. Muscarinic Type 1 Receptors Mediate Part of Nitric Oxide's Vagal Facilitatory Effect in the Isolated Innervated Rat Right Atrium. *Nitric Oxide - Biol. Chem.* **2007**, *16*, 110–117.

(36) Cabré, G.; Garrido-Charles, A.; Moreno, M.; Bosch, M.; Porta-de-la-Riva, M.; Krieg, M.; Gascón-Moya, M.; Camarero, N.; Gelabert, R.; Lluch, J. M.; Busqué, F.; Hernando, J.; Gorostiza, P.; Alibés, R. Rationally Designed Azobenzene Photoswitches for Efficient Two-Photon Neuronal Excitation. *Nat. Commun.* **2019**, *10*, 1–12.

(37) Araujo, D. M.; Lapchak, P. A.; Regenold, W.; Quirion, R. Characterization of [3H]AF-DX 116 Binding Sites in the Rat Brain: Evidence for Heterogeneity of Muscarinic-M2 Receptor Sites. *Synapse* **1989**, *4*, 106–114.

(38) Giachetti, A.; Micheletti, R.; Montagna, E. Cardioselective Profile of AF-DX 116, a Muscarine

M2 Receptor Antagonist. *Life Sci.* **1986**, *38*, 1663–1672.

(39) Shrestha, R.; Mohammed, S. K.; Hasan, M. M.; Zhang, X.; Wahid, K. A. Automated Adaptive Brightness in Wireless Capsule Endoscopy Using Image Segmentation and Sigmoid Function. *IEEE Trans. Biomed. Circuits Syst.* **2016**, *10*, 884–892.

(40) Feiner, R.; Engel, L.; Fleischer, S.; Malki, M.; Gal, I.; Shapira, A.; Shacham-Diamand, Y.; Dvir, T. Engineered Hybrid Cardiac Patches with Multifunctional Electronics for Online Monitoring and Regulation of Tissue Function. *Nat. Mater.* **2016**, *15*, 679–685.

(41) Yamamura, H. I.; Snyder, S. H. Muscarinic Cholinergic Binding in Rat Brain. *Proc. Natl. Acad. Sci. U. S. A.* **1974**, *71*, 1725–1729.

(42) Dörje, F.; Wess, J.; Lambrecht, G.; Tacke, R.; Mutschler, E.; Brann, M. R. Antagonist Binding Profiles of Five Cloned Human Muscarinic Receptor Subtypes. *J. Pharmacol. Exp. Ther.* **1991**, *256*, 727-733.

Table of Contents graphic

crypto-azologization of tricyclic ligands

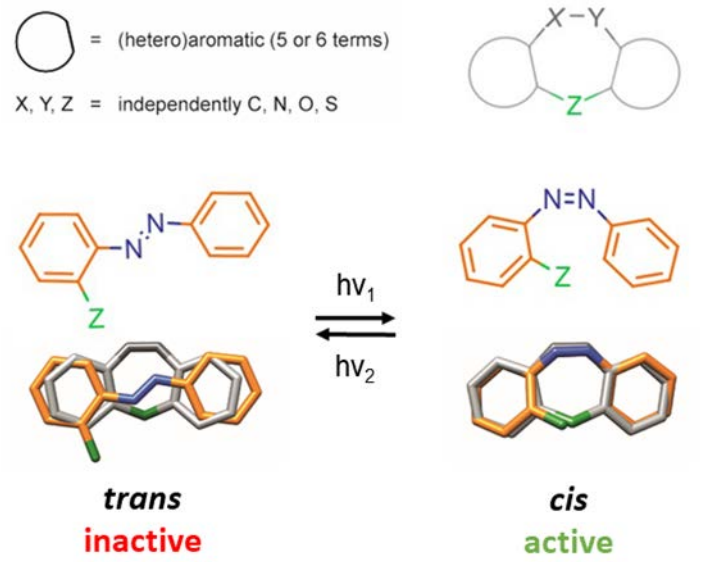

Supporting Information (*SI*)

Rational design of photochromic analogs of tricyclic drugs

Fabio Riefolo,[1,2,†] Rosalba Sortino,[1,2,‡] Carlo Matera,[1,2,3,‡] Enrique Claro,[4] Beatrice Preda,[1] Simone Vitiello,[1,¤] Sara Traserra,[5] Marcel Jiménez,[5,6] Pau Gorostiza[1,2,7,]*

[1] Institute for Bioengineering of Catalonia (IBEC), Barcelona Institute for Science and Technology (BIST), Barcelona 08028, Spain.

[2] Network Biomedical Research Center in Bioengineering, Biomaterials, and Nanomedicine (CIBER-BBN), Madrid 28029, Spain.

[3] Department of Pharmaceutical Sciences, University of Milan, Milan 20133, Italy.

[4] Institut de Neurociències and Departament de Bioquímica i Biologia Molecular, Unitat de Bioquímica de Medicina, Universitat Autònoma de Barcelona (UAB), Barcelona 08193, Spain.

[5] Department of Cell Biology, Physiology and Immunology, Universitat Autonoma de Barcelona, Barcelona 08193, Spain.

[6] Centro de Investigación Biomédica en Red de Enfermedades Hepáticas y Digestivas (CIBERehd), Instituto de Salud Carlos III, Madrid 28029, Spain.

[7] Catalan Institution for Research and Advanced Studies (ICREA), Barcelona 08010, Spain.

‡ Equivalent contribution.

* E-mail: pau@icrea.cat

† Present address: Teamit Research, Barcelona Health Hub, Barcelona 08025, Spain.

¤ Present address: Department of Life Sciences, University of Modena and Reggio Emilia, Via Campi 103, 41125 Modena, Italy.

Contents

1. Molecular docking simulations

1.1 Materials and methods

Molecular docking simulations were performed using the crystal structure of the human M1 muscarinic acetylcholine receptor retrieved from the Protein Data Bank bound to the antagonist tiotropium (PDB code: 5CXV).[1] The protein pdb file was prepared for docking by removing co-crystallized ligands, non-complexed ions and water molecules, and finally applying the Dock Prep tool available in the free software package UCSF Chimera. This involved the addition of hydrogens and assigning partial charges (AMBER ff14SB method). The cryptozepine-2, *trans* and *cis*, structures were built with standard bond length and angles using ChemDraw and then energy minimized with Chem3D by the MM2 method. The minimized compounds were further prepared for docking studies with UCSF Chimera by adding hydrogens and assigning partial charges (AMBER ff14SB method). The necessary pdbqt files of ligands and receptor were prepared using AutoDock 4.2 software. The docking studies were carried out using the standard docking protocol applied for AutoDock Vina in PyRx 0.8 virtual screening software. Autodock Vina has been reported to be an effective tool capable of quickly and accurately predicting bound conformations and binding energies of ligands with macromolecular targets.[2,3] A grid box of size 18.68 × 17.35 × 13.64 Å, with x, y and z coordinates of –11.52, –12.61 and 37.05, respectively, was fixed to cover the entire orthosteric binding sites and accommodate the ligands to move freely. Docking studies were performed using an exhaustiveness value of 8 while all other parameters were maintained as defaults. All rotatable bonds within the ligands were allowed to rotate freely, and the receptor was considered rigid. The docking simulations were repeated three times for each ligand. The obtained poses were then ranked based on the predicted affinity docking scores (kcal/mol) and the best pose for each experiment was selected. The results were then analyzed using UCSF Chimera. Both isomers of the cryptozepine-2 and pirenzepine were docked into the orthosteric binding sites of the human M1 muscarinic acetylcholine receptor in its inactive conformation, bound to the antagonist tiotropium (PDB code: 5CXV). All the ligands were docked at this receptor model using a standard docking protocol with AutoDock Vina in the PyRx 0.8 software with a suitable grid box. We ran three/five simulations for each ligand isomer and selected the best pose obtained in each experiment based on the predicted binding affinity scores (kcal/mol).

1.2 Molecular docking simulations of cryptozepine isomers.

In order to examine if the “crypto-azologization” concept was a reasonable strategy for developing light-sensitive crypto-azologs of pirenzepine, we firstly used molecular docking calculations. We docked cryptozepine-**2**, the crypto-azolog of pirenzepine with the simplest unsubstituted azobenzene as molecular switch, into the orthosteric binding site of the human M_1 muscarinic acetylcholine receptor (inactive conformation bound to the antagonist tiotropium, PDB code: 5CXV).[1] We first validated the docking protocol with the parent compound pirenzepine. The obtained best poses and their average binding affinity (-8.3 kcal/mol) were in agreement with the results previously published for the same ligand (**Figure S1** panel **D**).[1] The key elements for antagonist binding at the M_1 receptor reside in the methylpiperazine amines.[1,4–6] This group must face and interact with the orthosteric site residues D105 and Y404 (transmembrane helices (TM) 3 and 7, respectively; residues are numbered according to the human M1 receptor sequence PDB number 5CXV) (**Figure S1**). Additional confirmation that pirenzepine adopts the correct orientation in our calculations is provided by the tricyclic core oriented as the aromatic portions of tiotropium, which is free to create hydrophobic contacts with Y106 (TM3), W157 (TM4) and Y381 (TM6) (**Figure S1**).[1] We next studied cryptozepine-**2** (**Figure S1**). Our calculations showed that the best poses of the *cis* isomer fit in the M_1 orthosteric site in a similar way to pirenzepine (**Figure S1**), with favorable binding affinity values (-9.1 kcal/mol) (**Figure S1**, panel **E**). In contrast, a flipped orientation was favored for the majority of the *trans* isomer poses (**Figure S1**, panel **F**), which are likely incompatible with antagonism activity.[1,4–6] The planar *trans* geometry of cryptozepine-2 covers a larger space with the aromatic portions (8.7 Å) than its bent *cis* isomer (6.9 Å) and pirenzepine (7.1 Å) (**Figure S1**). This may hinder the correct placing into the binding pocket of the rest of the ligand and result in loss of antagonist behavior. Thus, computational results were in agreement with the “crypto-azologization” concept and encouraged to pursue the synthesis of a small library of cryptozepines.

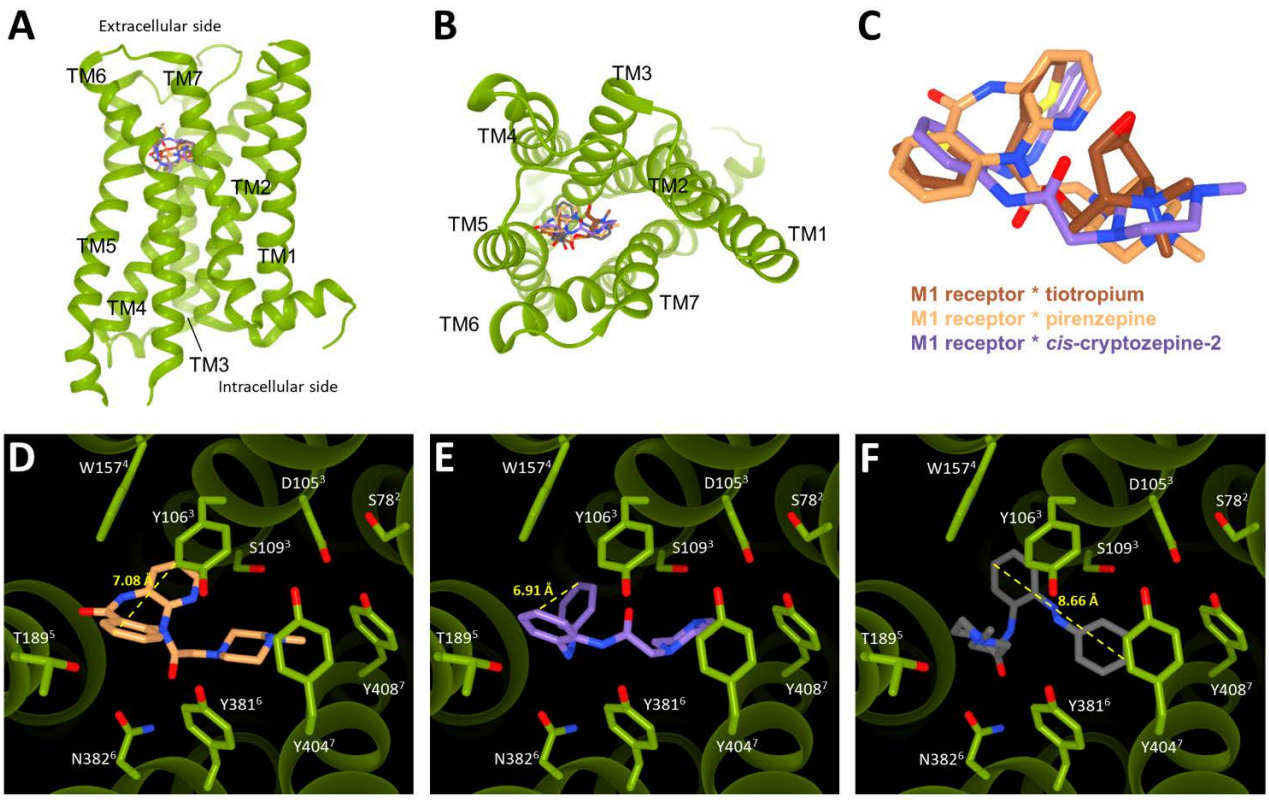

Figure S1. Hypothetical binding mode of cryptozepine-2 (trans and cis isomers) in M_1 mAChR. A and **B)** Full view (panel **A**) and extracellular side view (panel **B**) of the M_1 muscarinic structure (PDB code: 5CXV) colored in green, with our antagonists bound into the orthosteric site. **C**) Superimposition of binding poses of tiotropium from the M_1 structure (PDB code: 5CXV), pirenzepine, and the *cis*-cryptozepine-**2** from our simulations using the same receptor. **D**, **E** and **F**) Pirenzepine (panel **D**), *cis*- (panel **E**) and **trans**-cryptozepine-**2** (panel **F**) poses in the M_1 receptor with the fundamental residues that contribute to the orthosteric binding site (several residues are omitted for clarity). The ligands are shown as sticks and colored according to element: carbon, beige for pirenzepine, brown for tiotropium, purple for *cis*-cryptozepine-2, dark grey for *trans*-cryptozepine-2; oxygen, red; nitrogen, dark blue; sulfur, yellow. Residues are numbered according to the human M_1 receptor sequence (PDB code: 5CXV). Superscript numbers indicate the transmembrane (TM) helices of the M_1 receptor. The yellow line and values indicate the length of the tricyclic core of pirenzepine, and the aromatic portions of *trans*- and *cis*-cryptozepine-**2**. Pirenzepine and cryptozepine-**2** can antagonize CCh-induced bradycardia in mouse atria through M_1 receptors.

2. HPLC analyses and Mass Spectra

HPLC analyses were performed with a Waters Alliance 2795 separation module (RP column: XSelect CSH C18, 50x4.6 mm, S-3.5 µm, 1.6 ml/min; eluent: from 5% B to 100% B in 3.5 min using a linear gradient, A: H_2O 0.1% formic acid, B: acetonitrile 0.1% formic acid) coupled to a Waters 2996 photodiode detector and a Waters 3100 mass spectrometer (positive ionization analyses). PDA detector from 210 to 800 nm. Each HPLC analysis of the compounds has been superimposed to the corresponding blank analysis (solvent). Photoswitchable azobenzene-based compounds exist as an equilibrium between the two photoisomers (*trans* and *cis*). The equilibrium between the two photoisomers changes depending on the light conditions the compound is exposed to. This change can be detected by the HPLC diode array analyses where the two photoisomers, if thermodynamically stables, can be separated and measured as reported in the corresponding figures of this SI section. The confirmation that only the two photoisomers of the same compound are present is obtained by: a) the mass analyses of the two peaks, which remains equivalent, and, b) the continuous change of the two peaks' AU after different light exposures. All the compound purities are ≥ 95%, which is calculated as the sum of the *trans* and *cis* isomer peaks' AU. These levels of purity are confirmed also by HR-MS analyses, where the exact m/z of our compounds are detected. Characteristic “injection peaks” are present before 0.65 min due to the high Δ of pressure during the sample injection into the HPLC column.

2.1 Cryptozepine-1

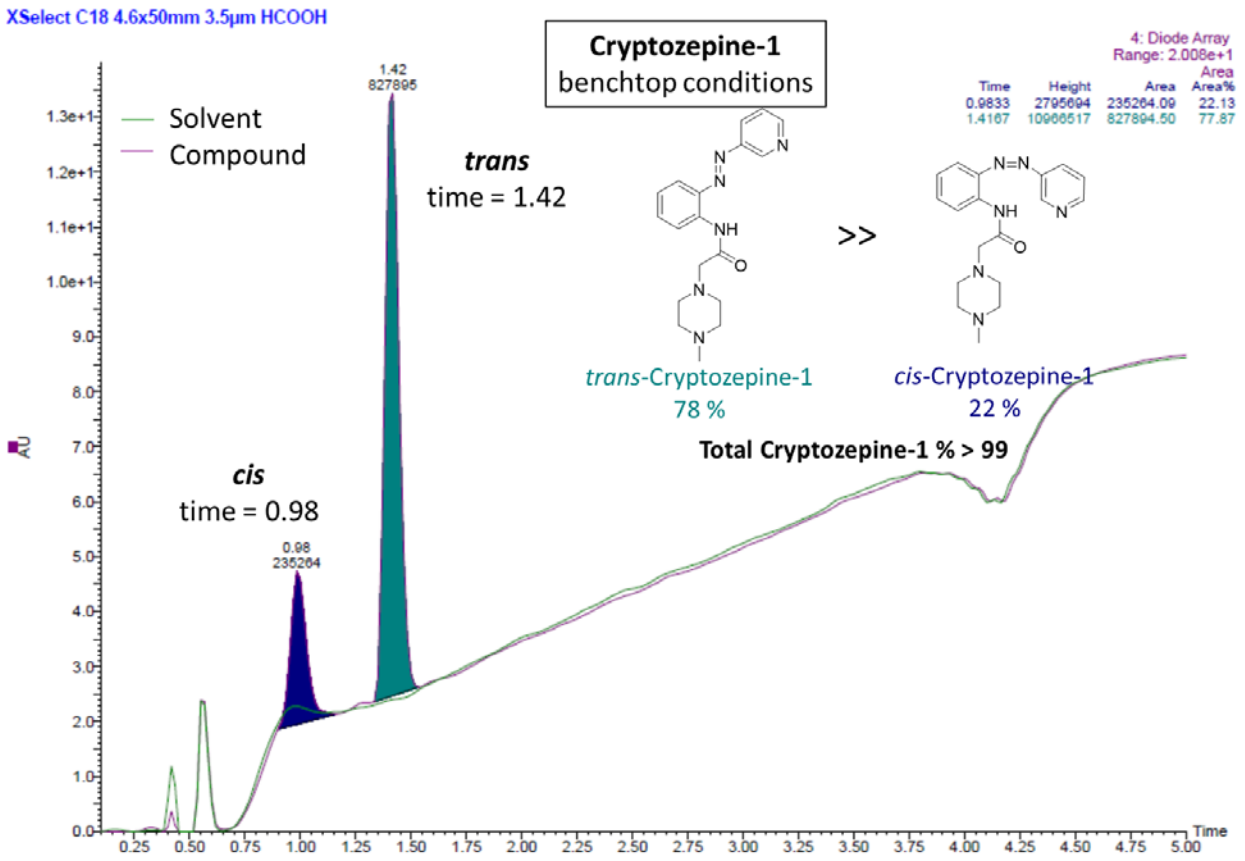

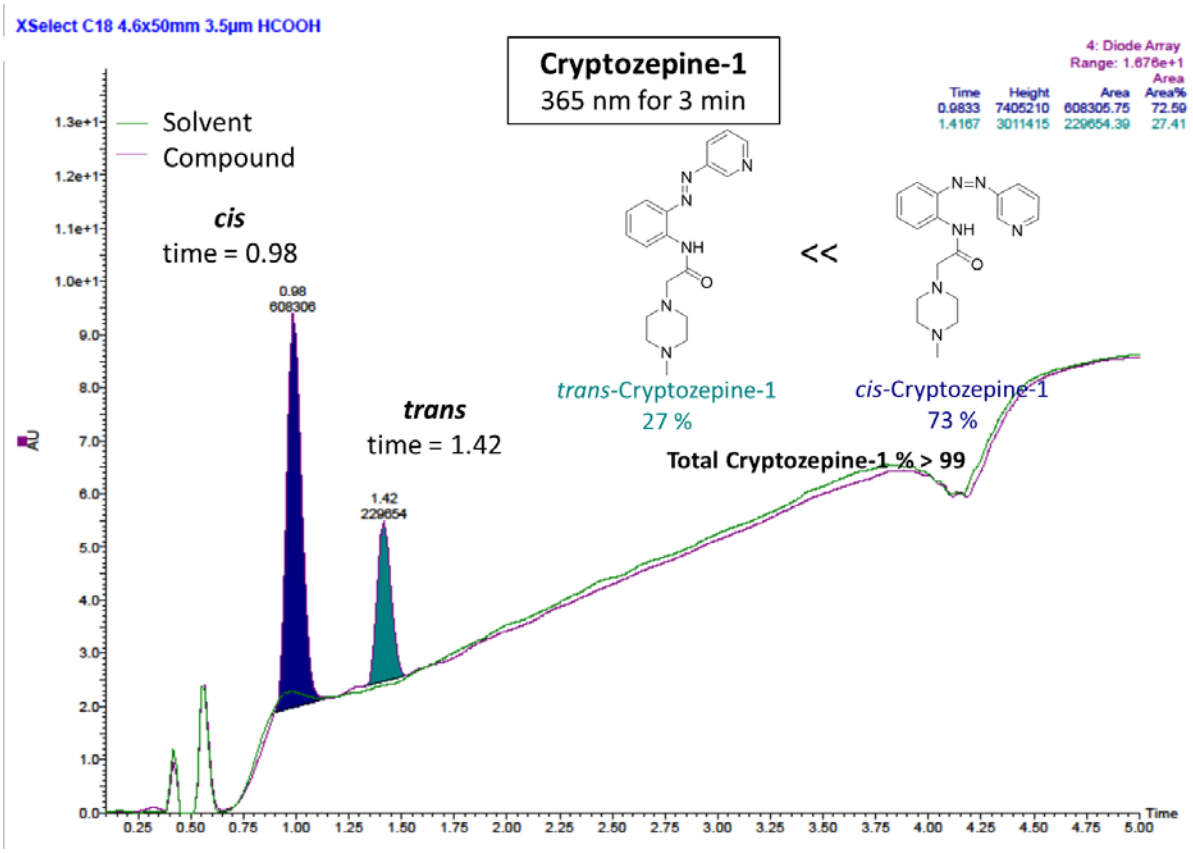

Cryptozepine-1

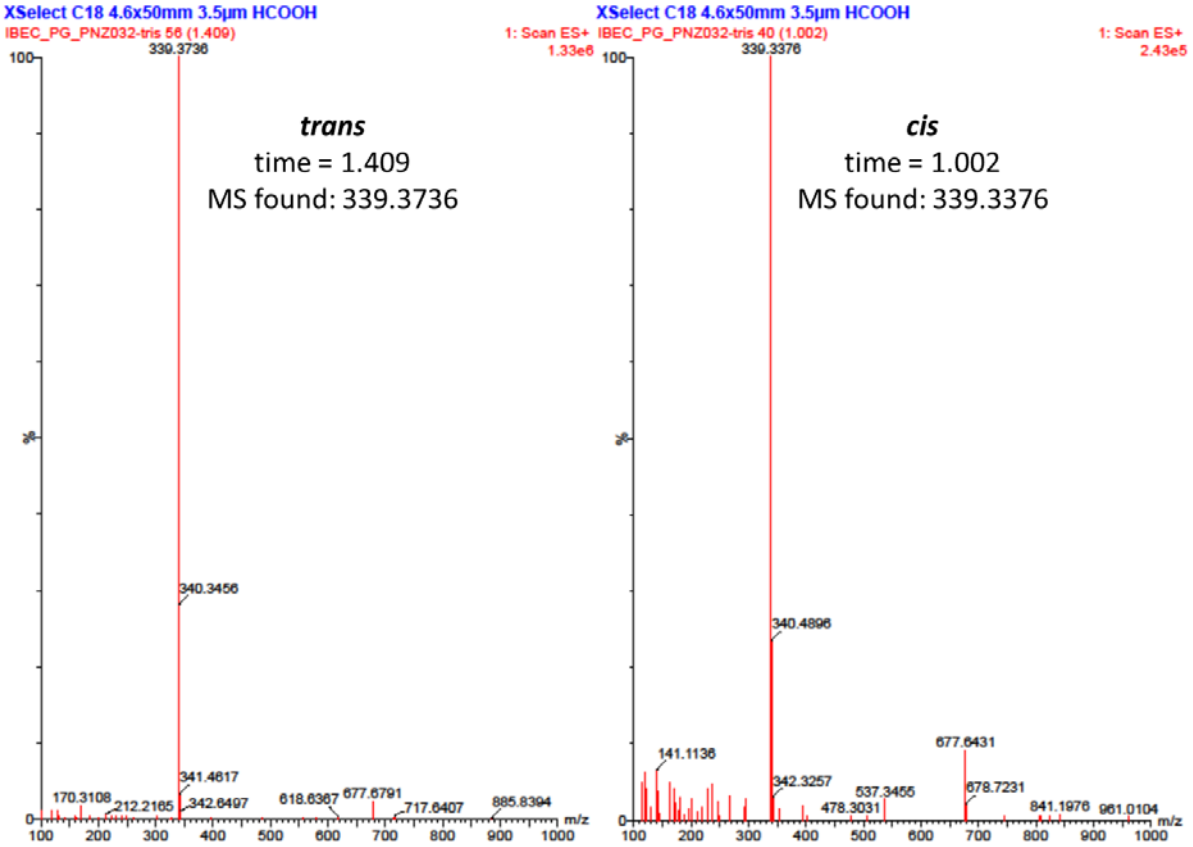

2.2 Cryptozepine-2

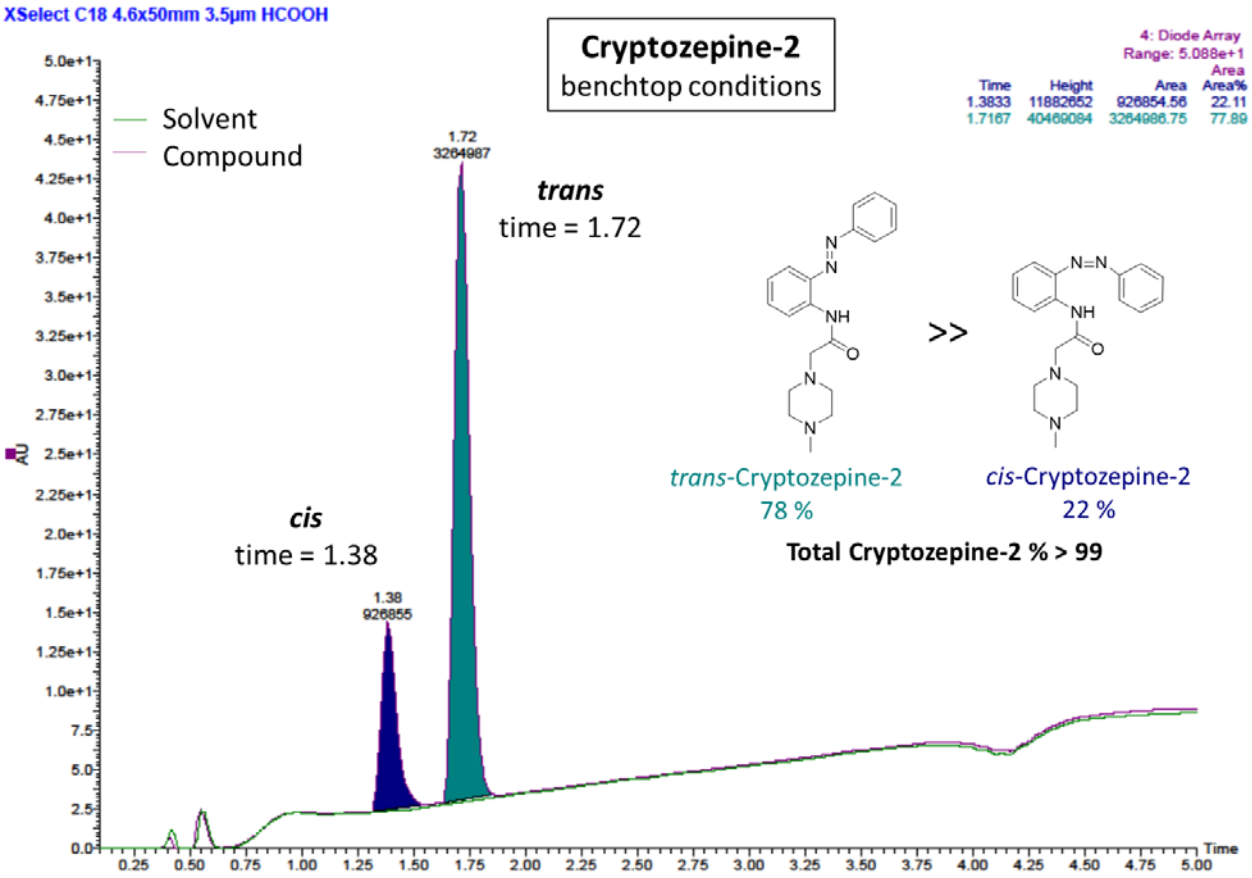

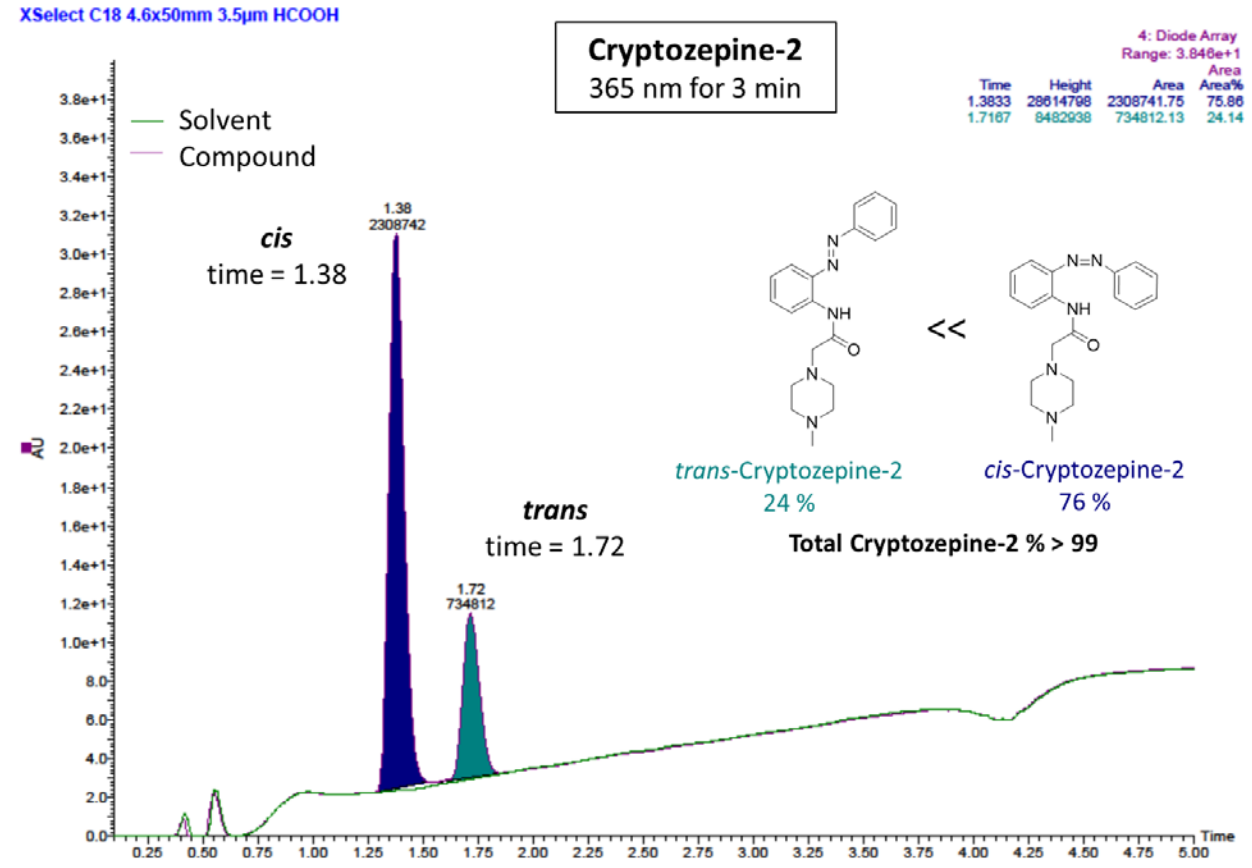

Cryptozepine-2

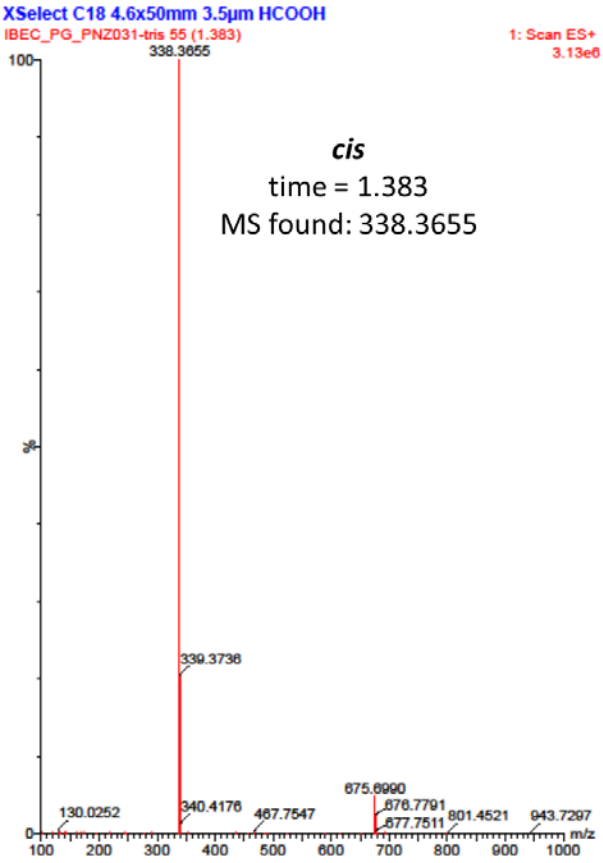

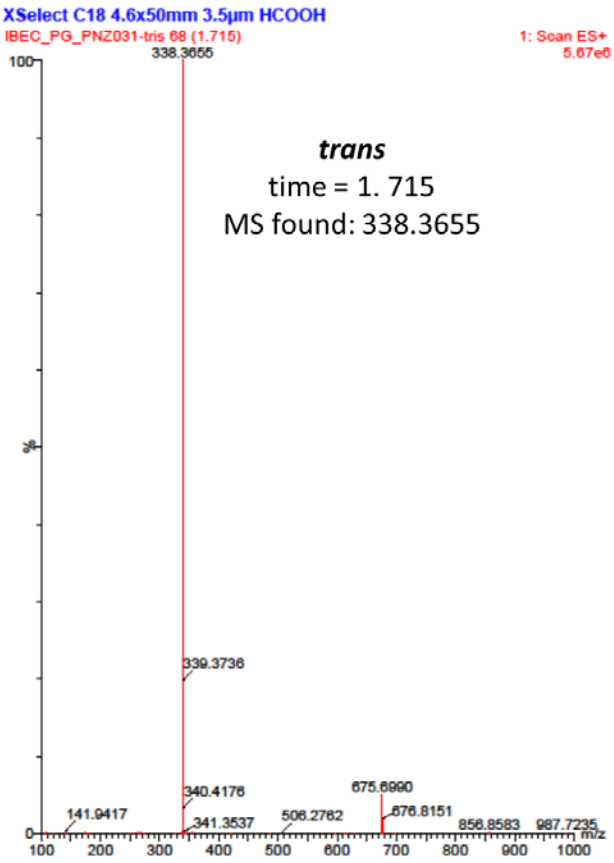

2.3 Cryptozepine-3

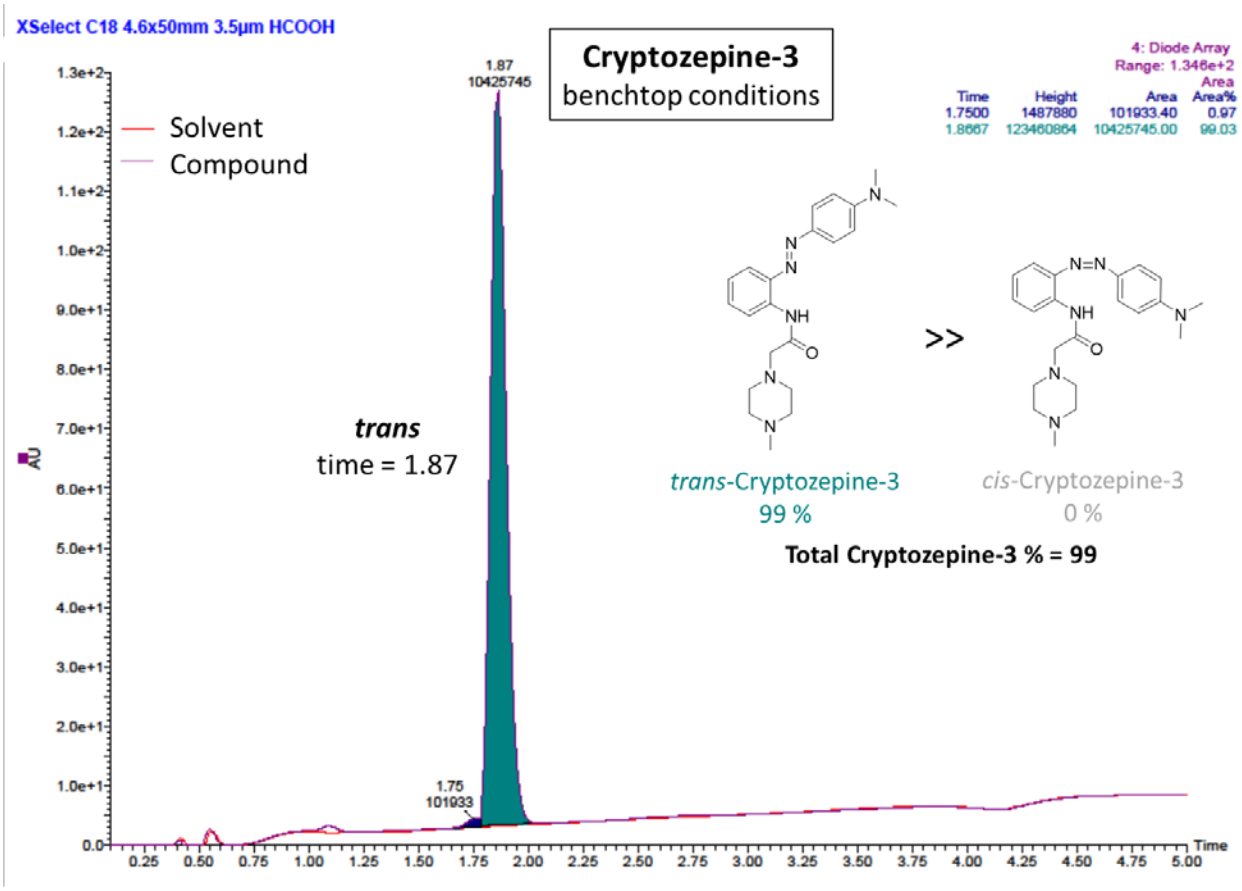

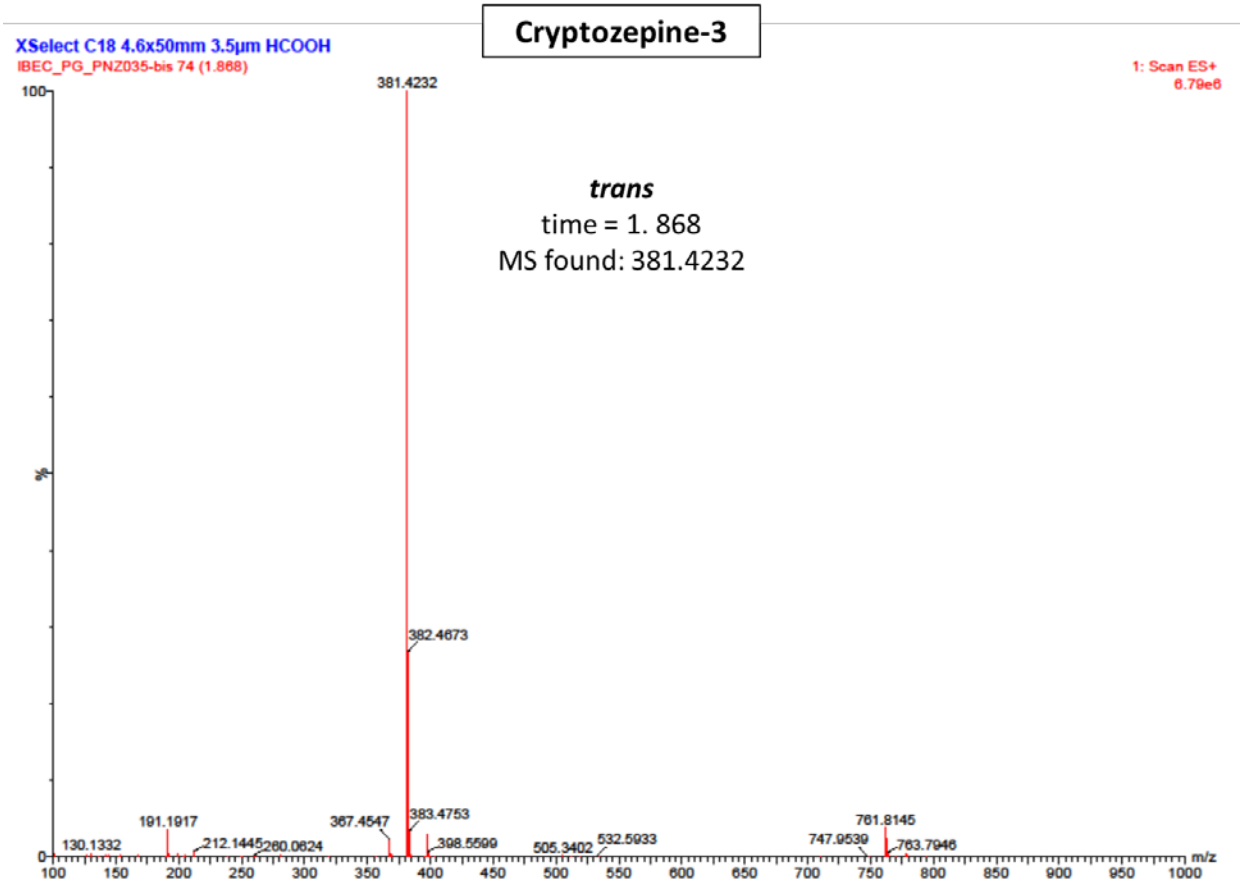

2.4 Cryptozepine-4

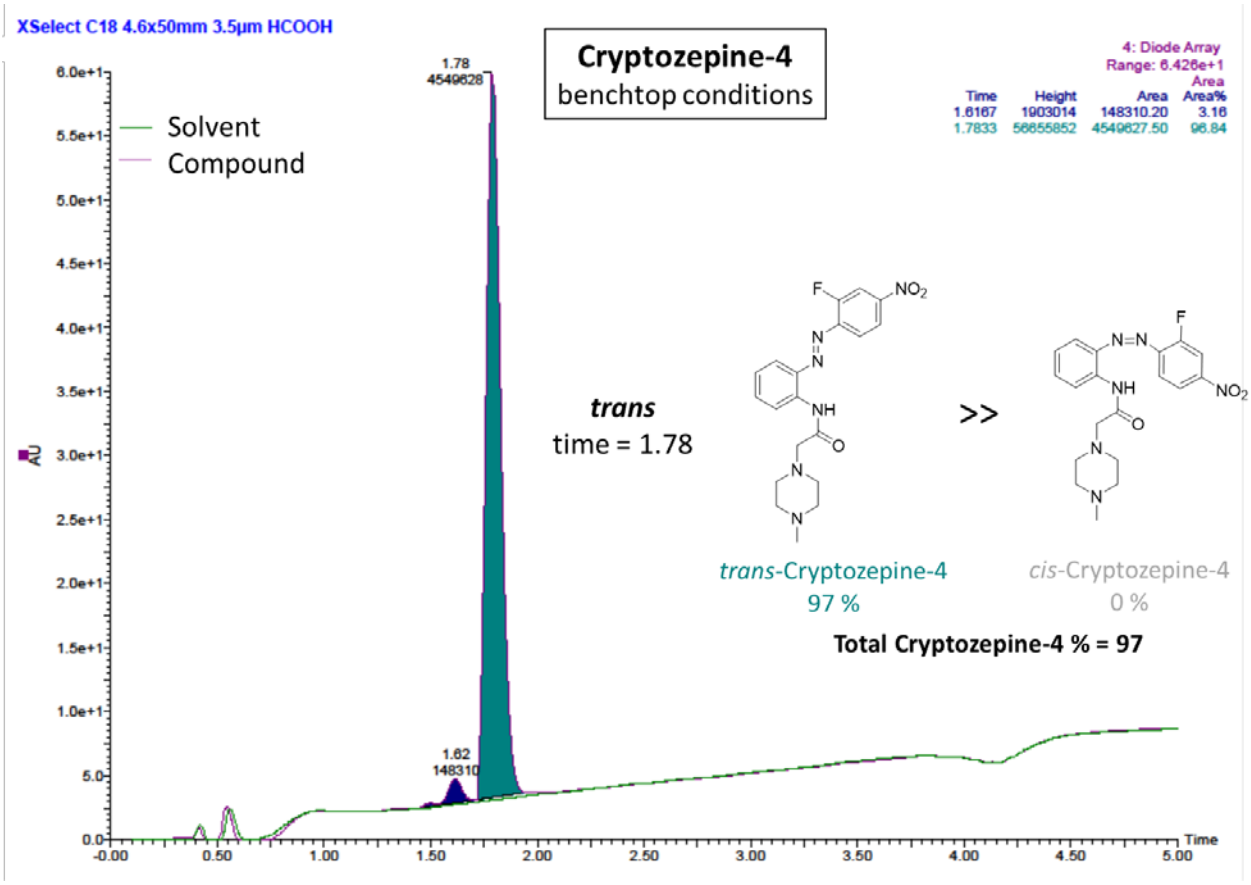

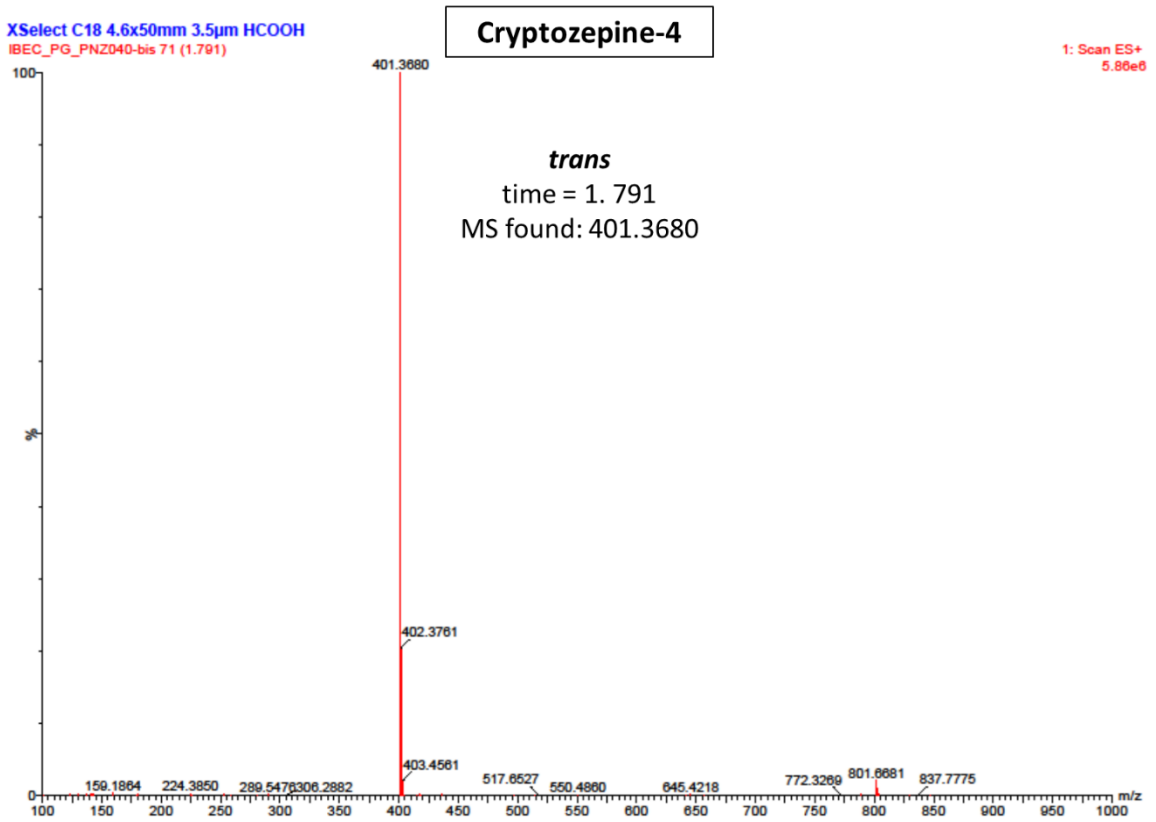

3. Photochemical characterization

An essential requirement for using our compounds as light-regulated M1 mAChRs antagonists is that they can effectively respond to light, which means that they can be quickly photoisomerized (from *trans* to *cis* and vice versa) between two different configurations with a relatively high degree of photoconversion (*trans*/*cis* ratio). We used UV-Vis spectroscopy and ^{1}H-NMR to characterize their photochromic behavior.

3.1 Cryptozepine-1

Cryptozepine-1 revealed a clear photochromic behavior with the typical absorption bands of azobenzenes. Maximum absorption peaks in aqueous solution were observed at around 315 nm and 430 (π–π* and n–π* transitions, respectively) (**Figure S3.1**, panel **B**). Cryptozepine-1 can be effectively isomerized from *trans* to *cis* with ultraviolet light (365 nm), and back-isomerized from *cis* to *trans* with white (WL) or blue (460 nm) light. The process is reversible and can be repeated several times without any noticeable loss of photochromic behavior (**Figure S3.1**, panel **D**). We estimated a half-life of thermal relaxation of about 71 min at 37 °C in the dark for the *cis* isomer (30 µM in water) obtained after illumination with 365 nm light (**Figure S3.1**, panel **C**).

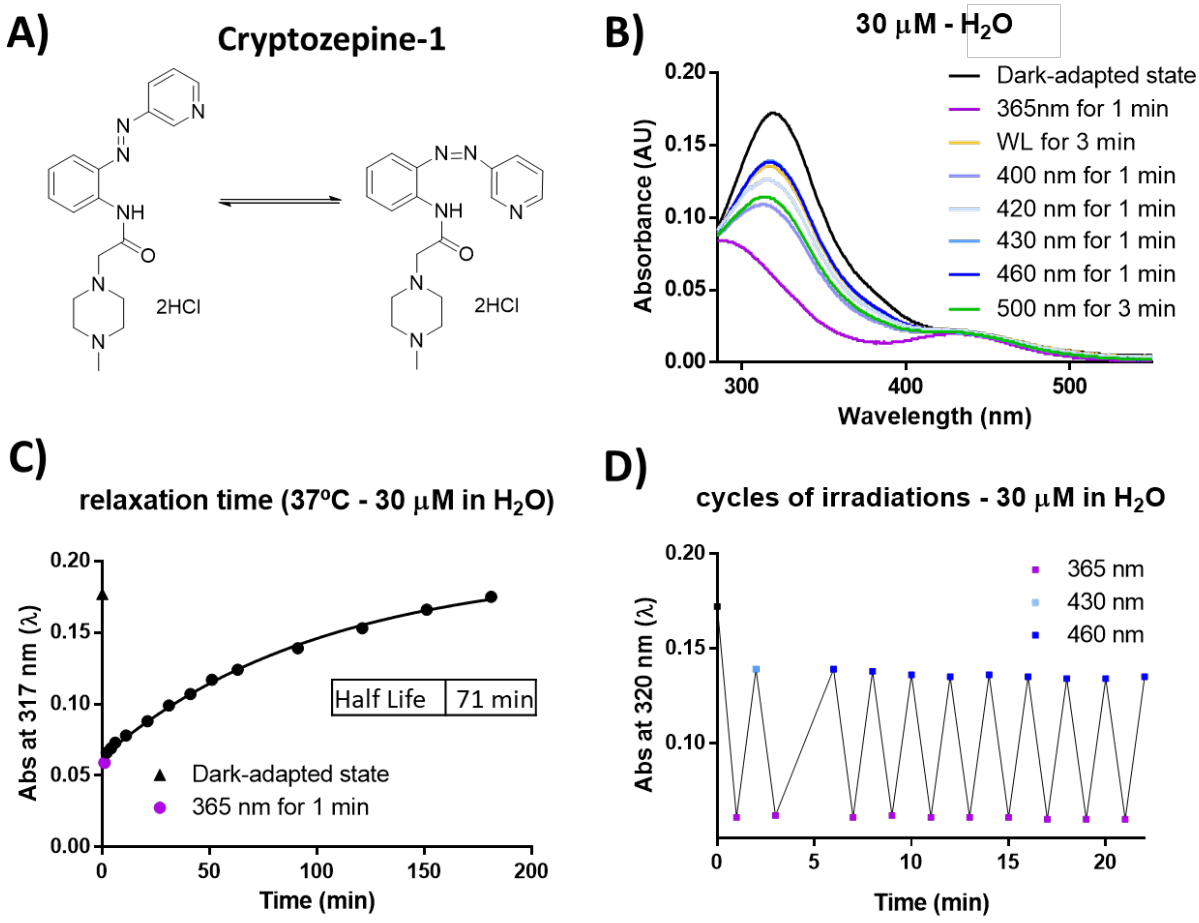

Figure S3.1. Photochemical characterization of cryptozepine-1. (**A**) Chemical structure of cryptozepine-1. (**B**) Absorption spectra in H_2O (30 µM). (**C**) Thermal stability: the photostationary state achieved after irradiation with 365 nm light in aqueous solution (30 µM) at 37 °C in the dark reverts to its dark-adapted state in less than 200 min. (**D**) Reversibility and stability of the photochromic behavior over several cycles of isomerization.

We next quantified by ^{1}H-NMR the extent of photoisomerization for cryptozepine-1 (1 mM in D_2O) (**Figure S3.1.1**). The amount of the thermodynamically less stable *cis* isomer shifted from an initial value of 19% (as obtained under benchtop conditions) to 87% upon irradiation with 365 nm light for 5 minutes. After irradiation at 460 nm (10 min), the *trans* form reverted to a 58%. In the dark-adapted state the amount of *trans* isomer was 91%.

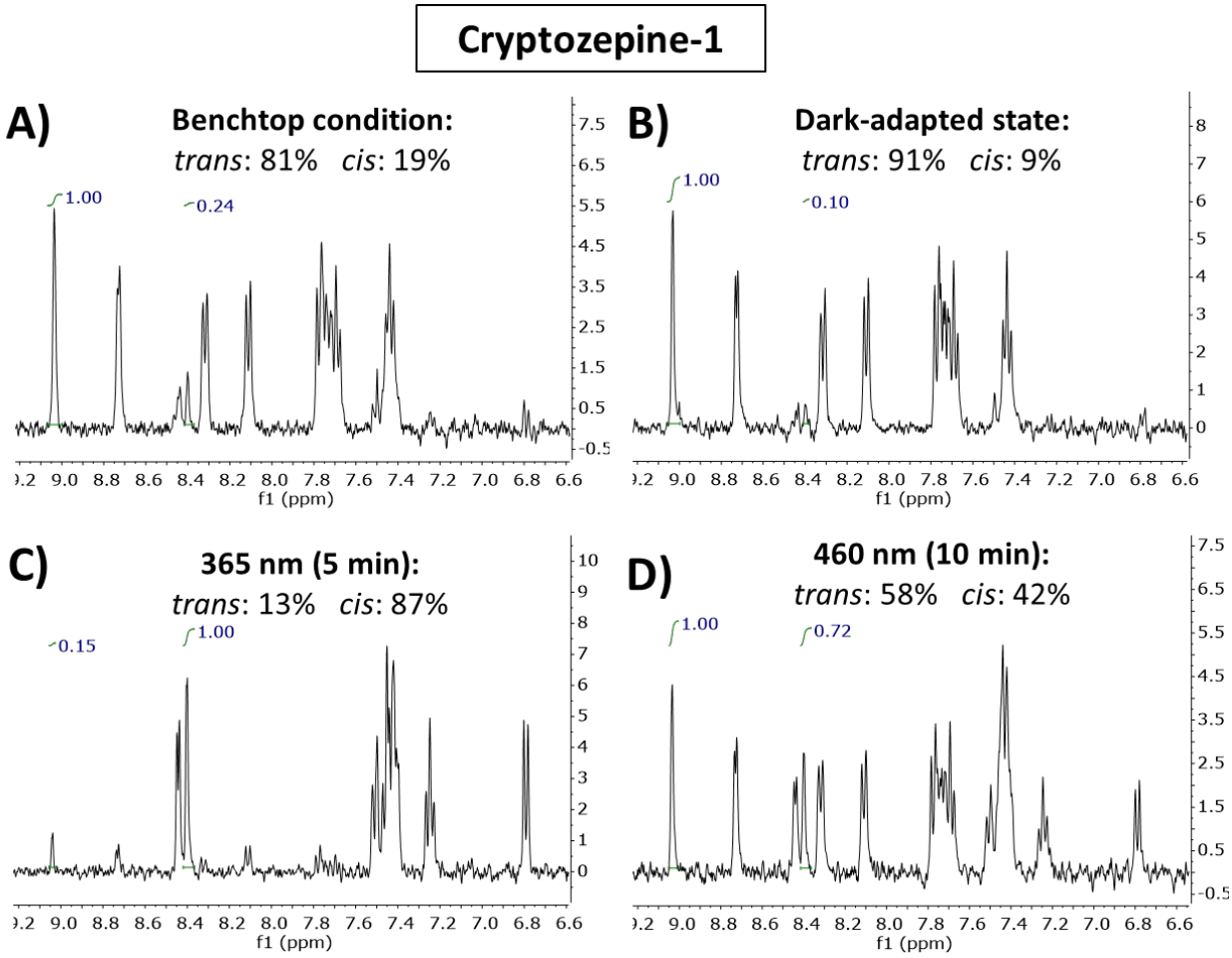

Figure S3.1.1 Quantification of the photostationary state of cryptozepine-1. (**A**) benchtop conditions, (**B**) dark-adapted state, (**C**) after 5 min of illumination with 365 nm light, and (**D**) after 10 min of illumination with 460 nm light.

3.2 Cryptozepine-2

Cryptozepine-**2** revealed a clear photochromic behavior with the typical absorption bands of azobenzenes. Maximum absorption peaks in aqueous solution were observed at around 315 nm and 430 nm (π–π* and n–π* transitions, respectively) (**Figure S3.2**, panel **B**). Cryptozepine-**2** can be effectively isomerized from *trans* to *cis* with ultraviolet light (365 nm), and completely back-isomerized from *cis* to *trans* with white (WL), blue (400-460 nm) or green (500 nm) light. The process is reversible and can be repeated several times without any noticeable loss of photochromic behavior (**Figure S3.2**, panel **D**). We estimated a half-life of thermal relaxation of about 180 min at 37 °C in the dark for the *cis* isomer (30 µM in water) obtained after illumination with 365 nm light (**Figure S3.2**, panel **C**).

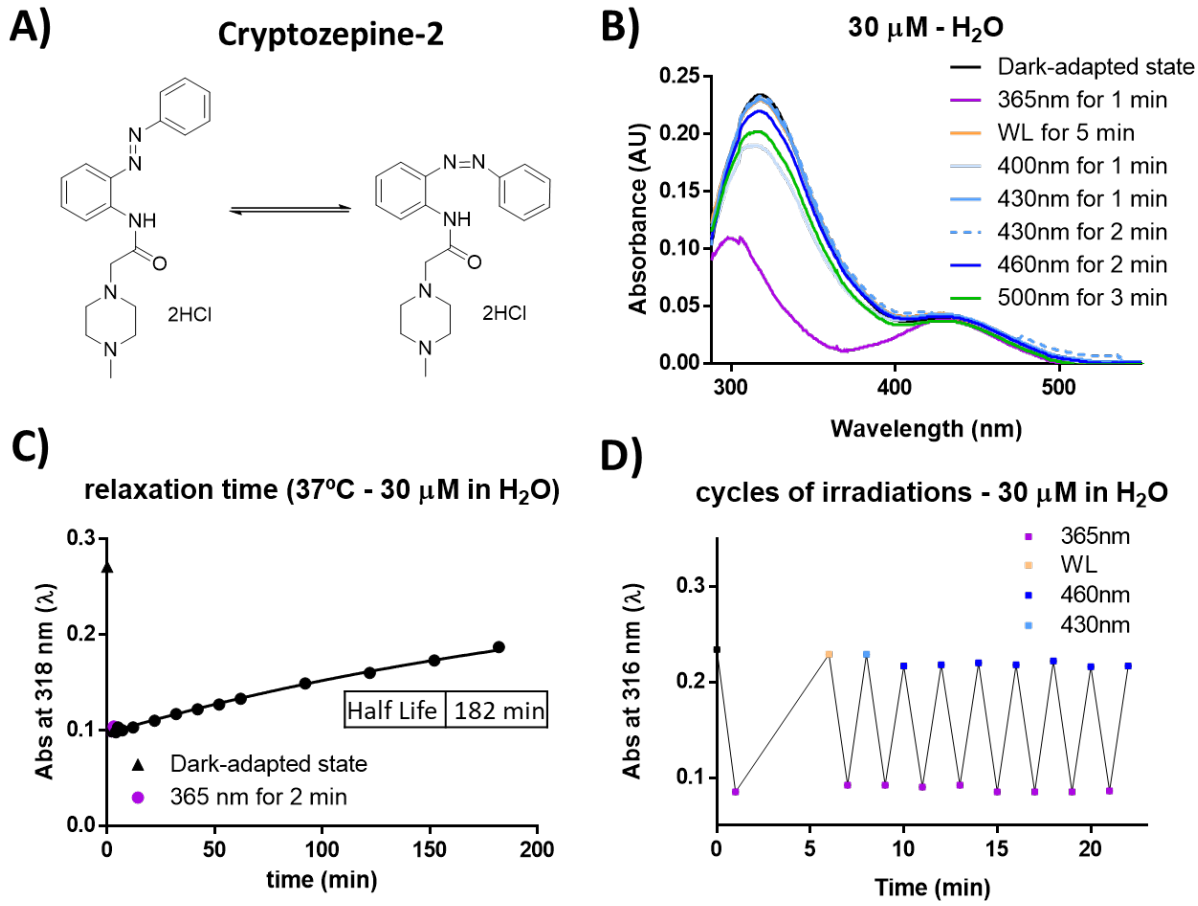

Figure S3.2. Photochemical characterization of cryptozepine-2. (**A**) Chemical structure of cryptozepine-2. (**B**) Absorption spectra in H_2O (30 µM). (**C**) Thermal stability: the photostationary state achieved after irradiation with 365 nm light in aqueous solution (30 µM) at 37 °C in the dark has a half-life of 182 min. (**D**) Reversibility and stability of the photochromic behavior over several cycles of isomerization.

We next quantified by ^{1}H-NMR the extent of photoisomerization for cryptozepine-**2** (1 mM in D_2O) (**Figure S3.2.1**). The amount of the thermodynamically less stable *cis* isomer shifted from an initial value of 7% (as obtained under benchtop conditions) to 90% upon irradiation with 365 nm light for 5 minutes.

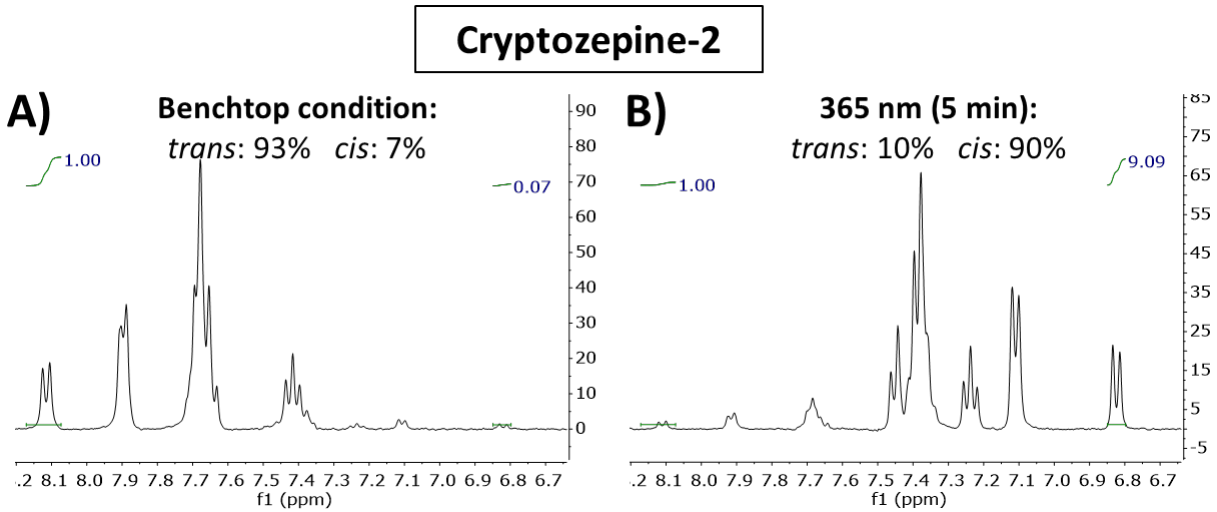

Figure S3.2.1 Quantification of the photostationary state of cryptozepine-2. (A) benchtop conditions, and (B) after 5 min of irradiation with 365 nm light.

3.3 Cryptozepine-3

Cryptozepine-**3** revealed a clear photochromic behavior with the typical absorption bands of push–pull azobenzenes. The absorbance of the *trans* isomer is red shifted by ~100 nm and greatly decreases the thermal stability of the *cis* isomer, so its photoisomerization cannot be observed by steady-state UV-vis spectroscopy in aqueous solution. Maximum absorption peak in anhydrous DMSO (30 µM) was observed at around 465 nm (**Figure S3.3**, panel **B**). Cryptozepine-**3** can be effectively isomerized from *trans* to *cis* with blue (420-460 nm) and green (500 nm) light. The photostationary state achieved after irradiation with red lights reverts in 20 min at 37 °C in anhydrous DMSO in the dark (**Figure S3.3**, panel **B**).

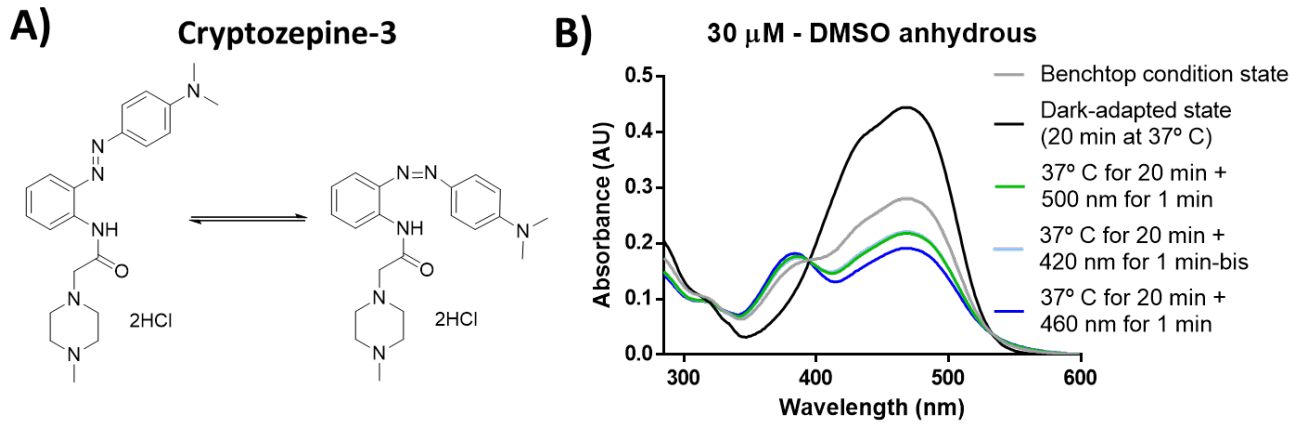

Figure S3.3. Photochemical characterization of cryptozepine-3. (**A**) Chemical structure of cryptozepine-**3**. (**B**) Absorption spectra in anhydrous DMSO (30 µM).

3.4 Cryptozepine-4

Cryptozepine-**4** revealed a clear photochromic behavior with the typical absorption bands of azobenzenes. Maximum absorption peaks in acidic water solution (pH 2) were observed at around 335 nm and 450 nm (π–π* and n–π* transitions, respectively) (**Figure S3.4**, panel **B**). Cryptozepine-**4** can be effectively isomerized from *trans* to *cis* with ultraviolet light (365-380 nm), and back-isomerized from *cis* to *trans* with blue light (420-460 nm). The process is reversible and can be repeated several times without any noticeable loss of photochromic behavior (**Figure S3.4**, panel **D**). We estimated a half-life of thermal relaxation of about 68 min at 37 °C in the dark for the *cis* isomer (30 µM, pH 2) obtained after illumination with 380 nm light (**Figure S3.4**, panel **C**).

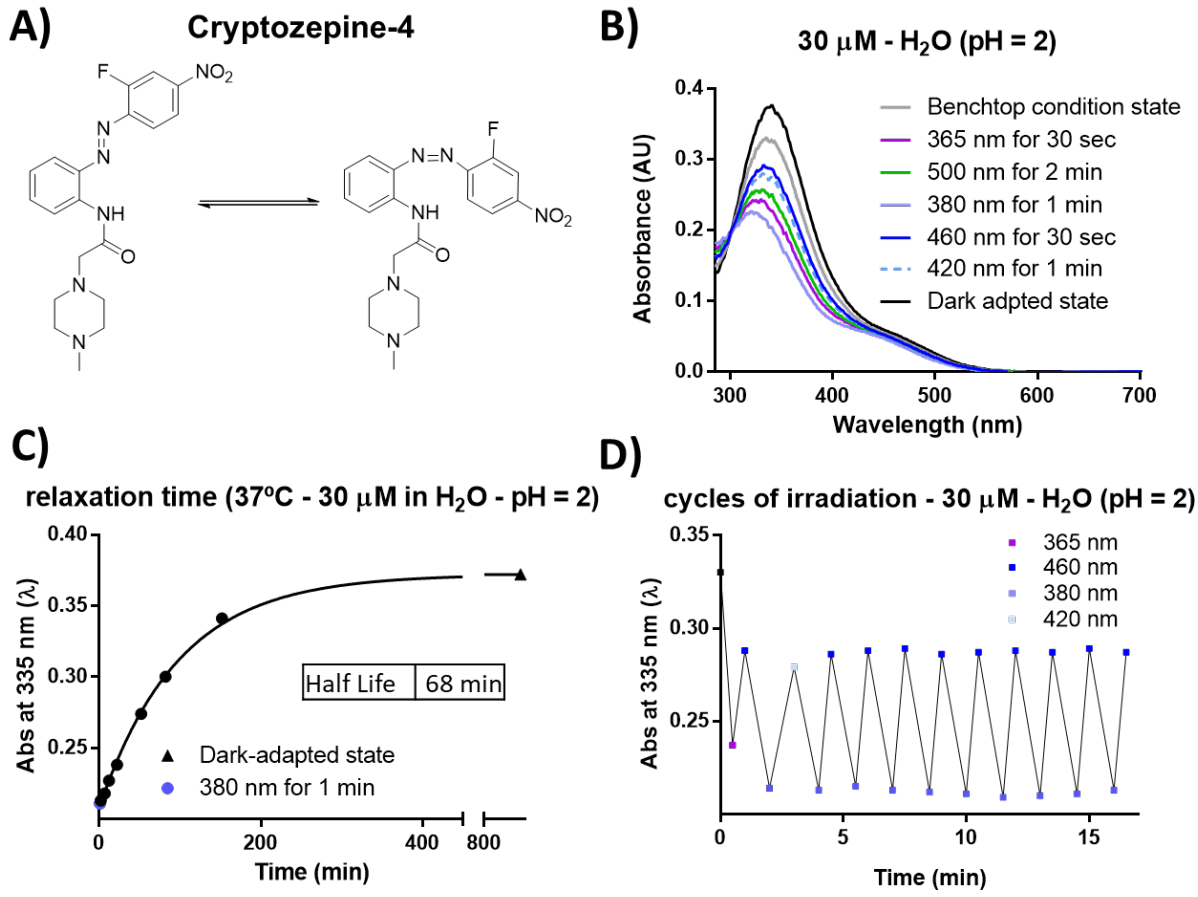

Figure S3.4. Photochemical characterization of Cryptozepine-4. (**A**) Chemical structure of Cryptozepine-**4**. (**B**) Absorption spectra in aqueous solution (30 µM, pH 2). (**C**) Thermal stability: the photostationary state achieved after irradiation with 380 nm light in aqueous solution (30 µM, pH 2) at 37 °C in the dark has a half-life of 68 min. (**D**) Reversibility and stability of the photochromic behavior over several cycles of isomerization.

We next quantified by ^{1}H-NMR the extent of photoisomerization for Cryptozepine-**4** (1.5 mM in D_2O + HCl, pH 2) (**Figure S3.4.1**). The amount of the *cis* isomer shifted from an initial value of 18% (benchtop conditions) to 61% upon irradiation with 380 nm light (10 min). After irradiation with 460 nm (10 min), the *trans* form reverted to a 67%. In the dark-adapted state the amount of the *trans* isomer was about 93%.

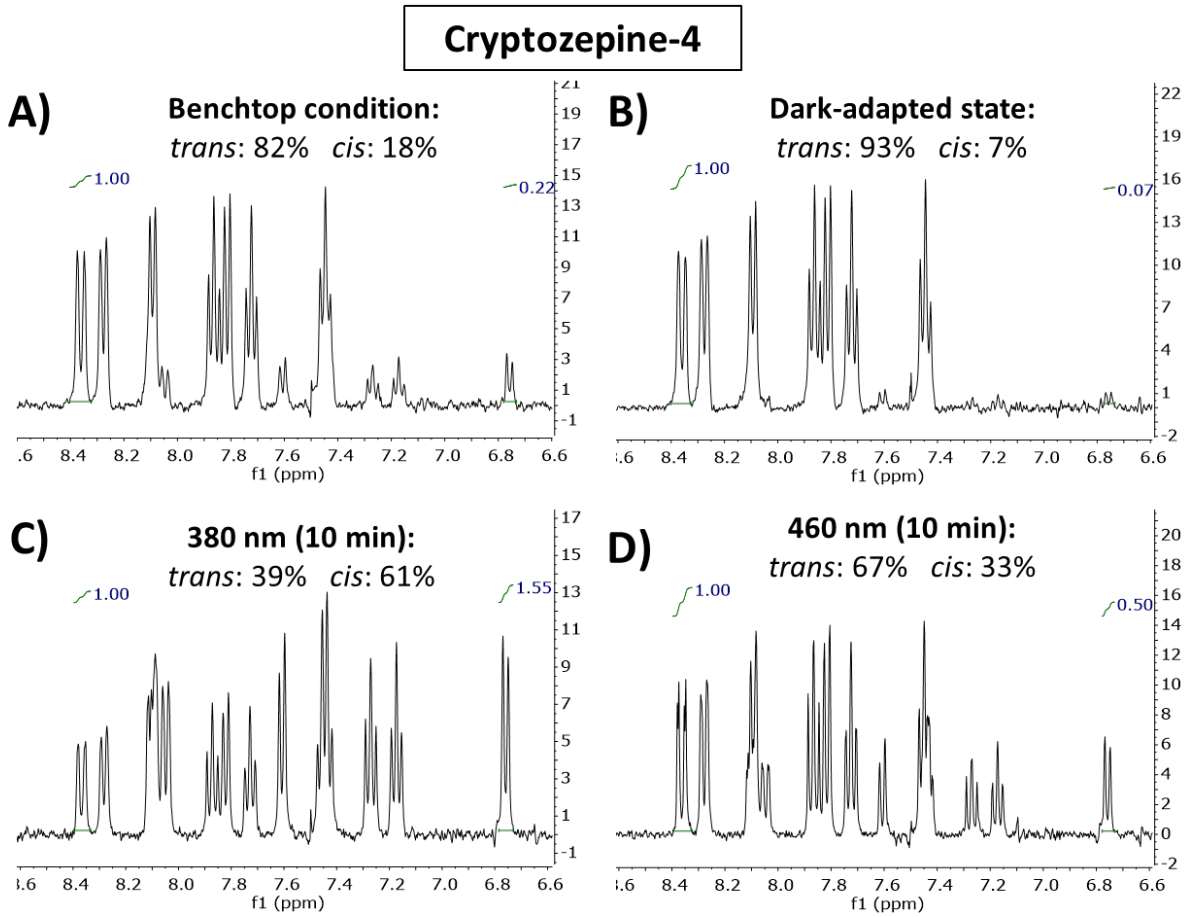

Figure S3.4.1 Quantification of the photostationary state of Cryptozepine-4. (**A**) benchtop conditions, (**B**) dark-adapted state, (**C**) after 10 min of irradiation with 380 nm light, and (**D**) after 10 min of irradiation with 460 nm light.

4. NMR spectroscopy

4.1 NMR spectra of cryptozepine-1

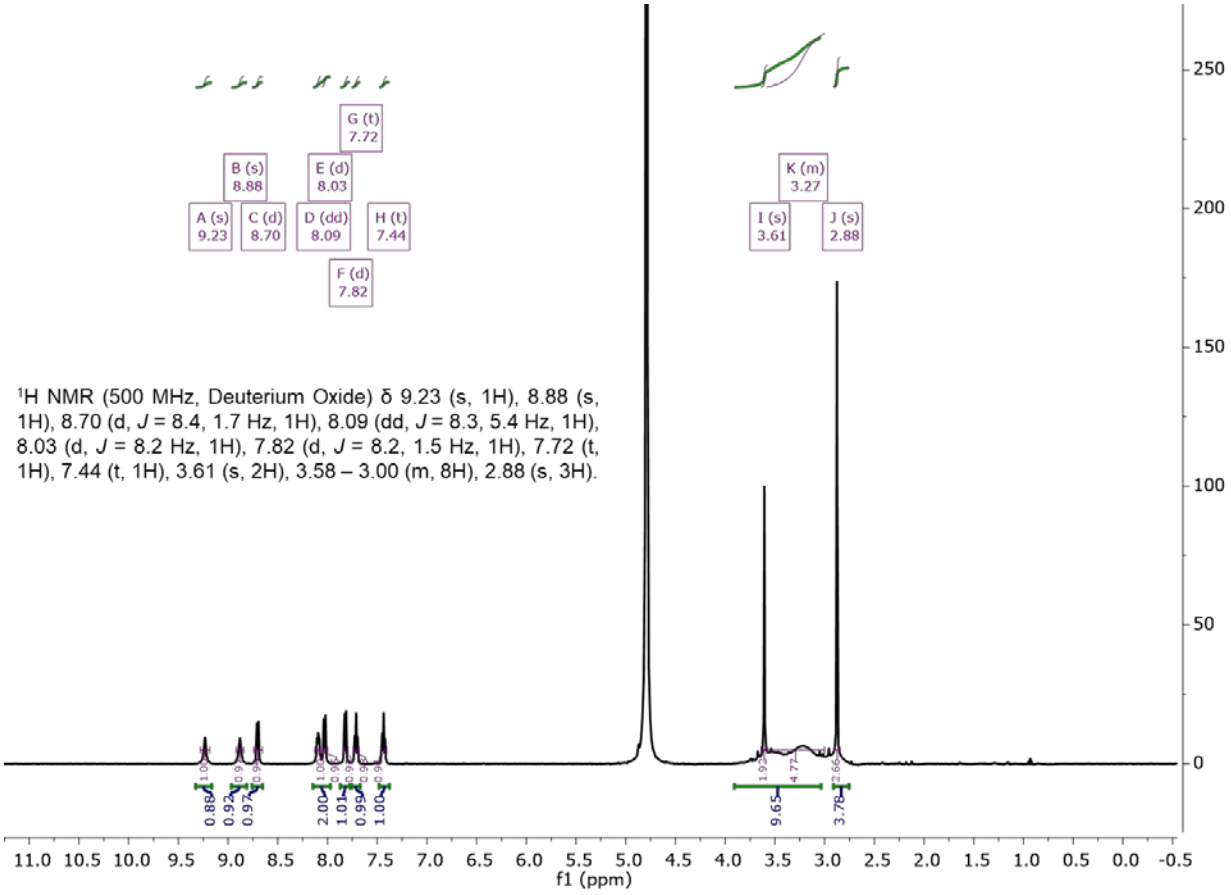

Figure S4.1. [1]H-NMR of cryptozepine-1 as obtained under benchtop conditions.

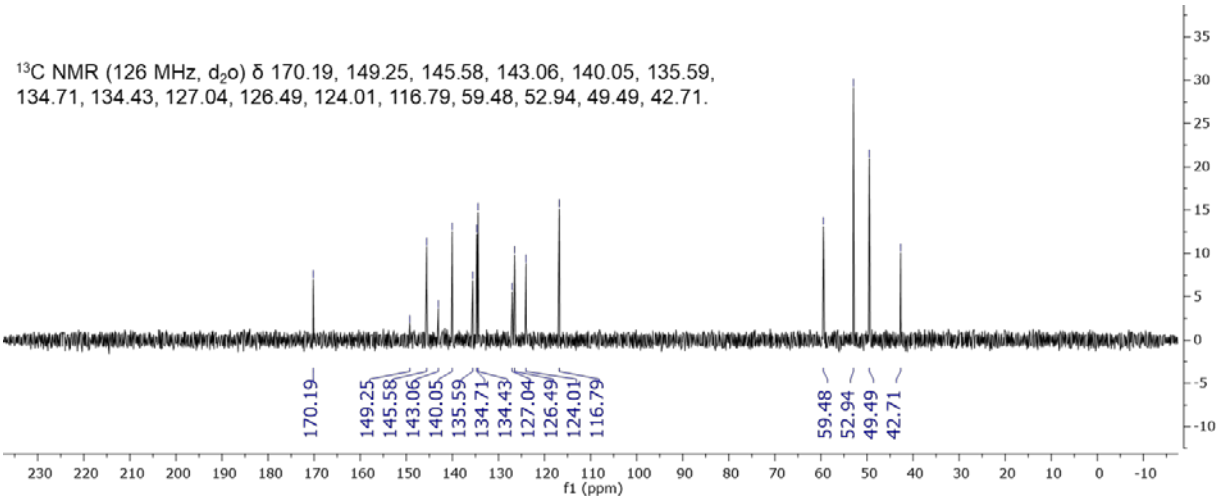

Figure S4.1.1 [13]C-NMR of cryptozepine-1 as obtained under benchtop conditions.

4.2 NMR spectra of cryptozepine-2

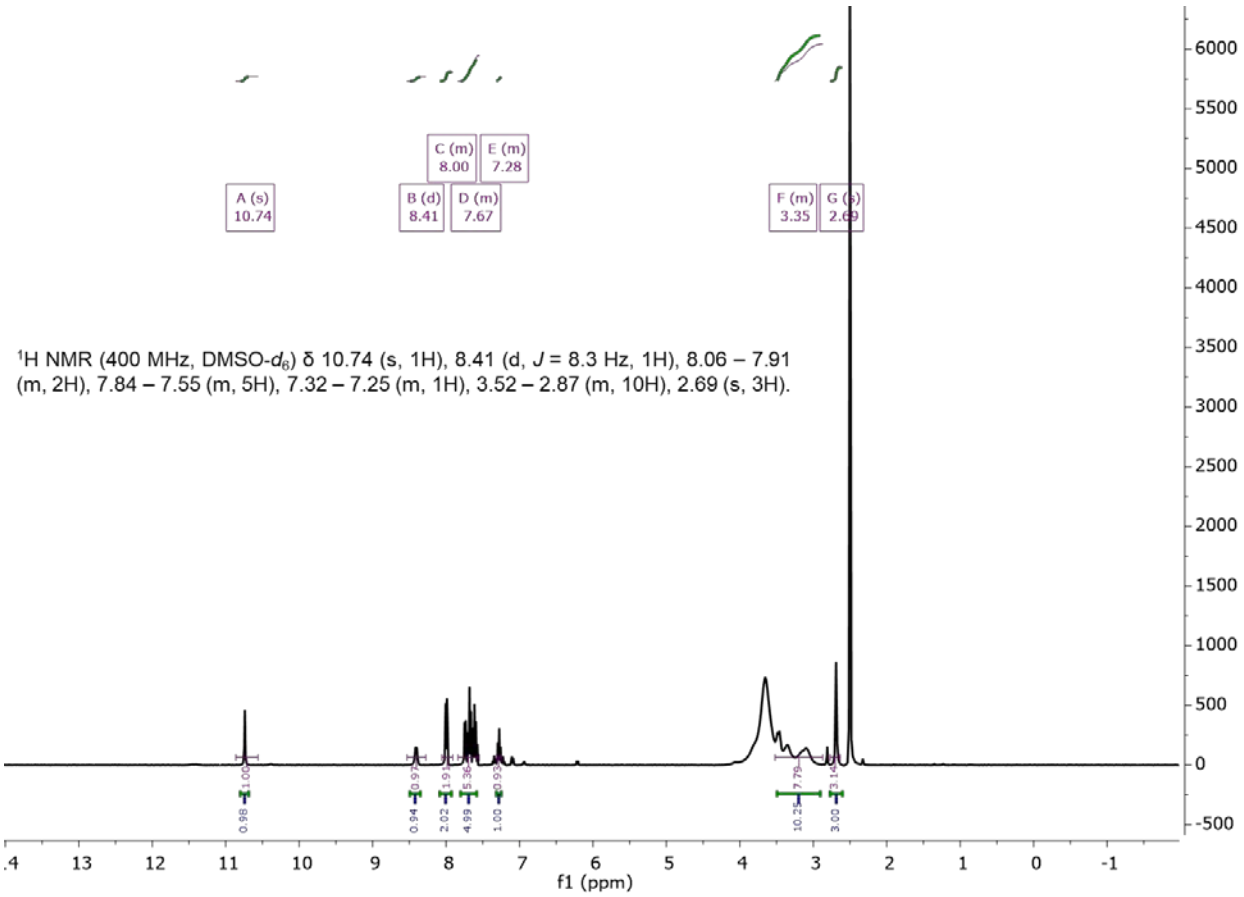

Figure S4.2 [1]H-NMR of cryptozepine-2 as obtained under benchtop conditions.

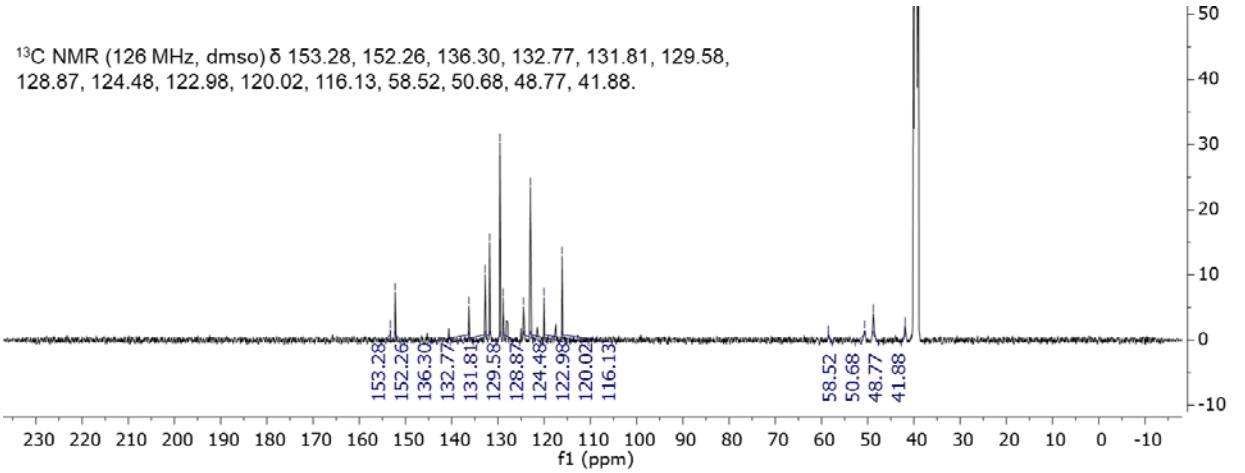

Figure S4.2.1 [13]C-NMR of cryptozepine-2 as obtained under benchtop conditions.

4.3 NMR spectra of cryptozepine-3

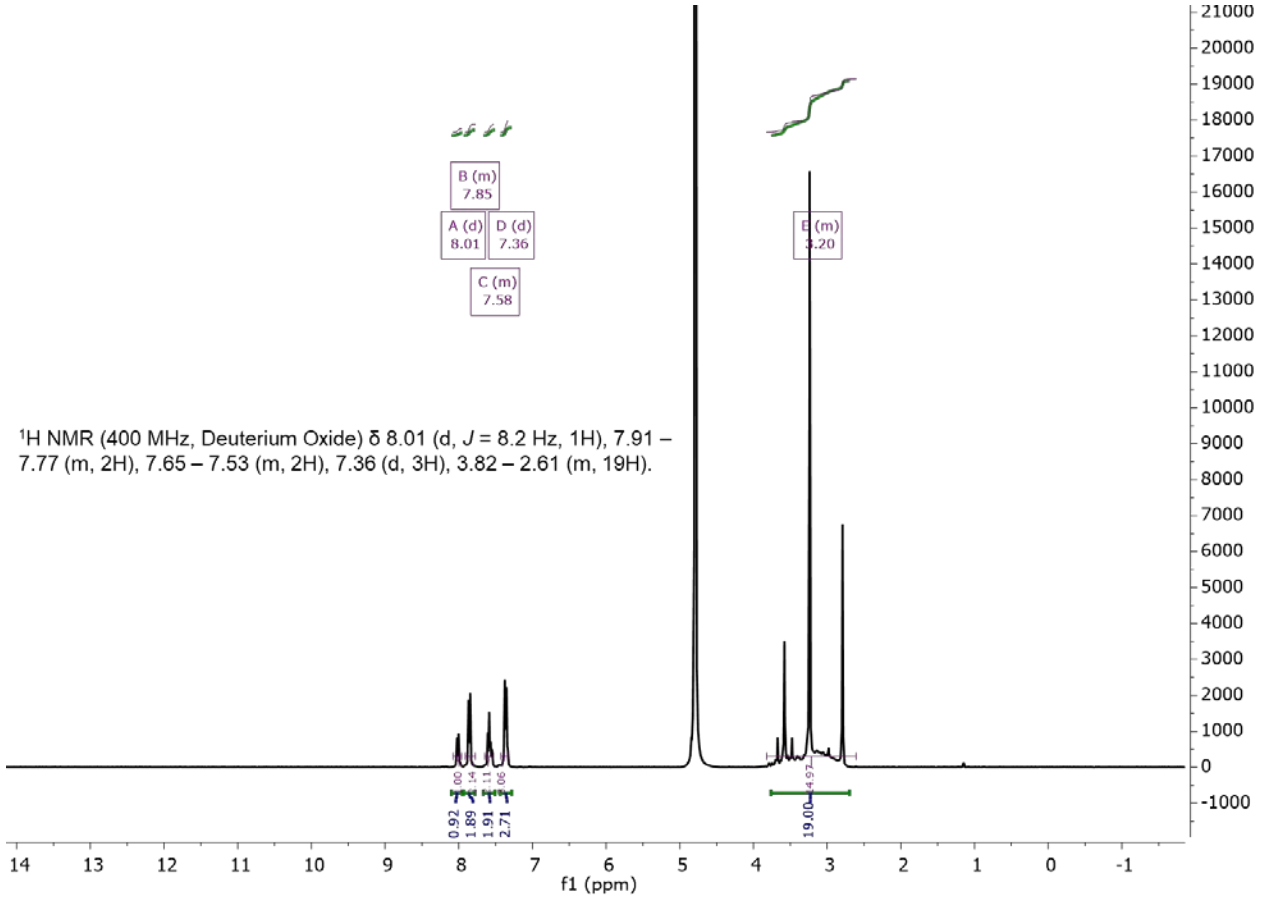

Figure S4.3 [1]H-NMR of cryptozepine-3 as obtained under benchtop conditions.

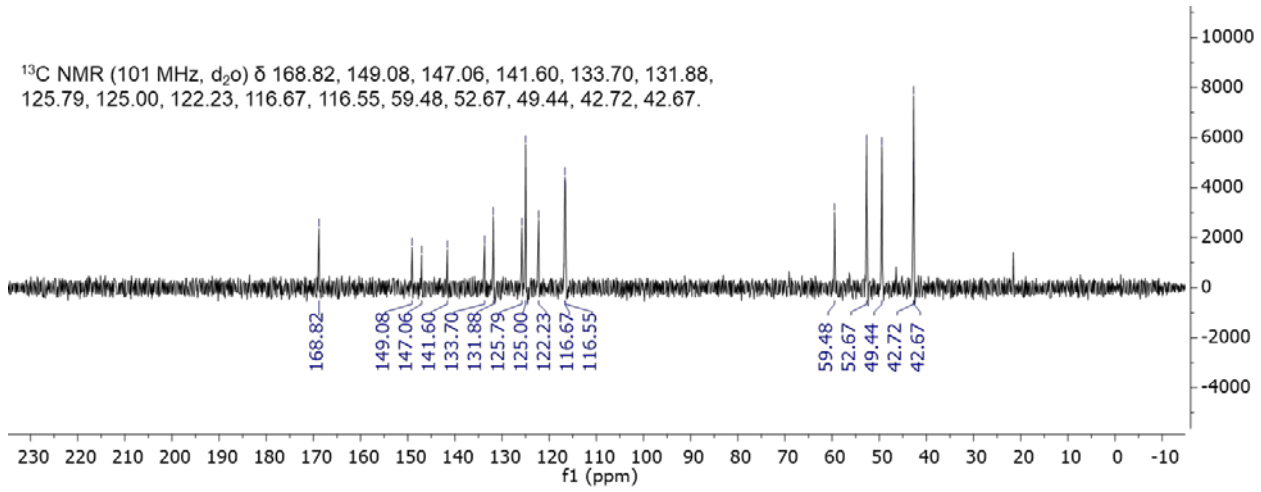

Figure S4.3.1 [13]C-NMR of cryptozepine-3 as obtained under benchtop conditions.

4.4 NMR spectra of cryptozepine-4

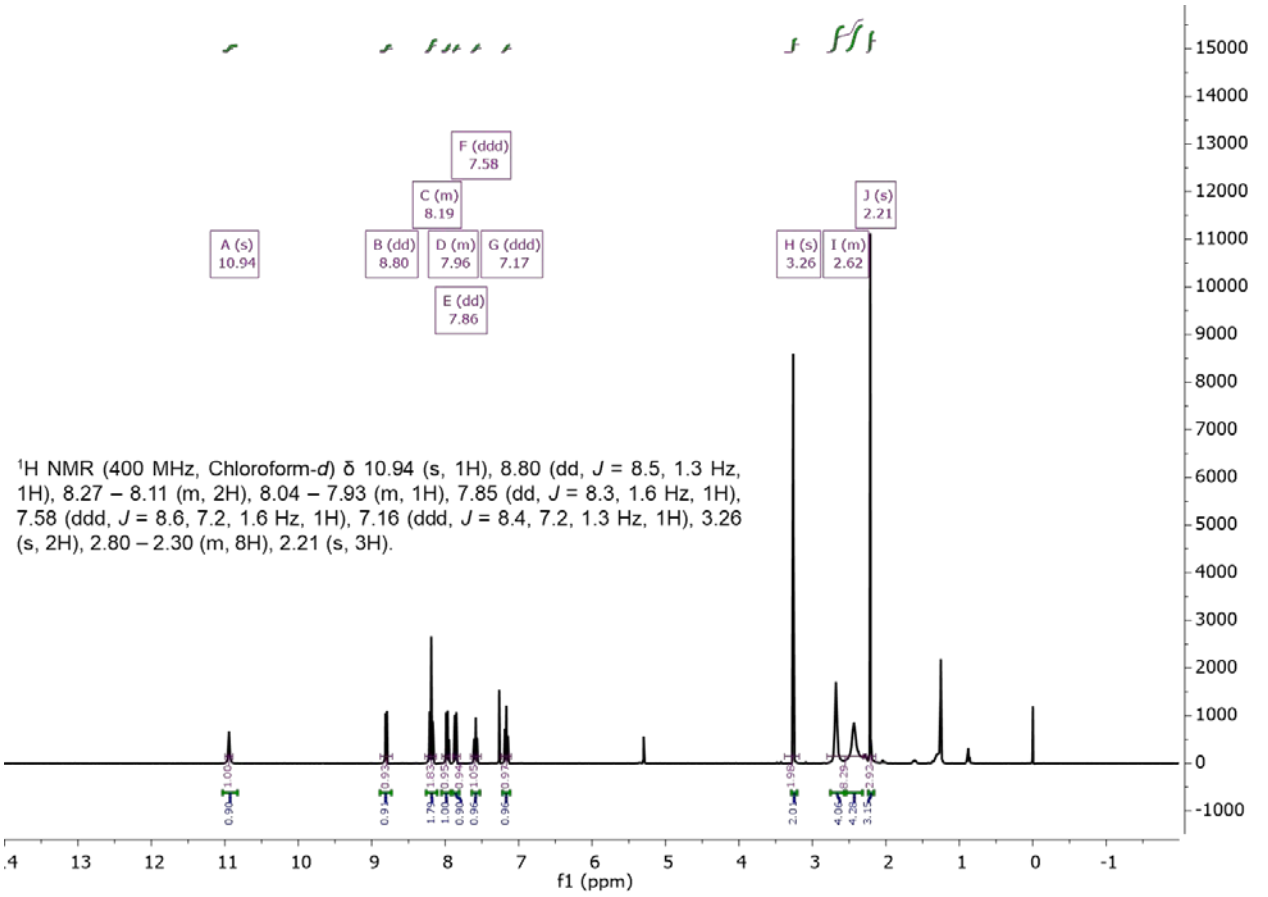

Figure S4.4 ^{1}H-NMR of cryptozepine-**4** as obtained under benchtop conditions.

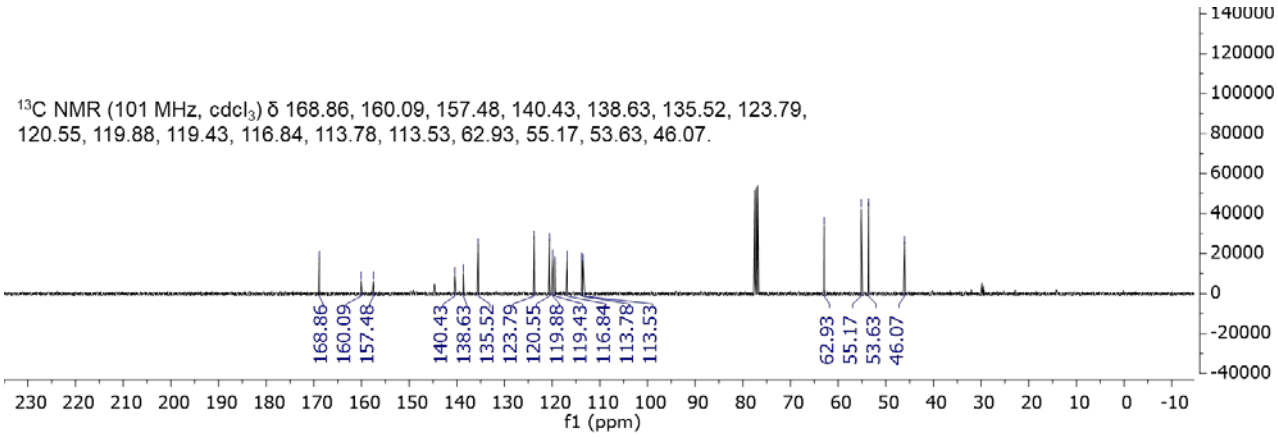

Figure S4.4.1 ^{13}C-NMR of cryptozepine-**4** as obtained under benchtop conditions.

5. *In vitro* radioligand competition binding experiments

5.1. *In vitro* radioligand competition binding experiments

The affinity of our compounds and pirenzepine (PNZ) for mAChRs was studied by radioligand competition binding experiments (see the **Experimental Section**).

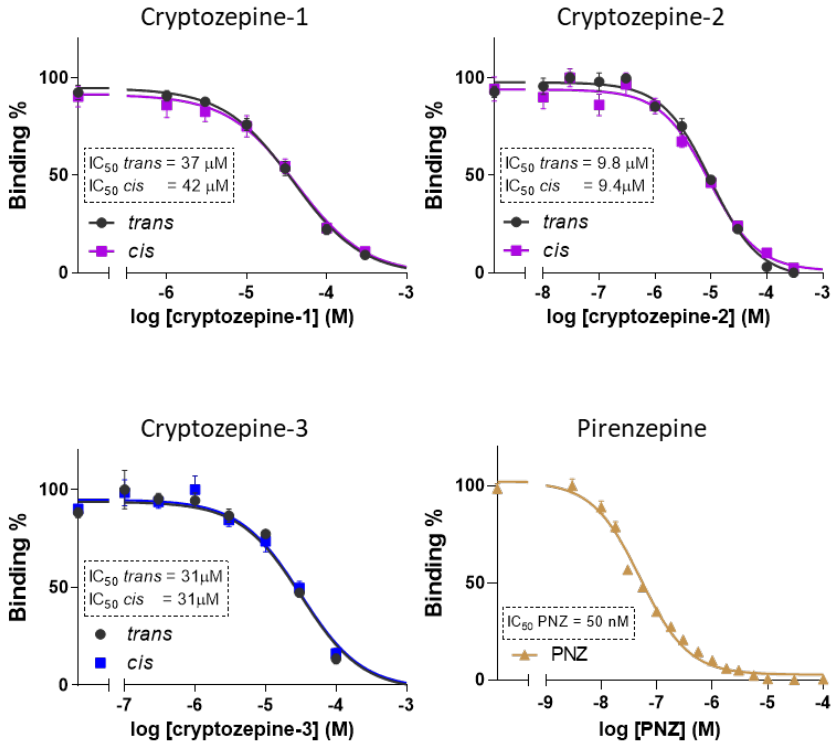

Figure S5.1. Competitive displacement of specific radioligand binding from mAChRs. Competition for specific binding of 200 pM [^{3}H]QNB to 3-4 months-old female Wistar rats brain membranes (whole cortex) containing high density of all five mAChRs by cryptozepines-**1**, **2**, **3** and pirenzepine (PNZ) (n = 4 for each isomer of cryptozepines and n = 2 for PNZ). Data points were fitted using the "Binding – Competitive – one site - Fit Ki" for Ki values, and "Binding – Competitive – one site - Fit logIC50" for the IC_{50}, which are functions in GraphPad Prism 6. Values are means ± SEM.

5.2. In vitro specific M1 and M2 muscarinic binding assays study of *cis*-Cryptozepine-2

The *in vitro* radioligand binding assay of 1, 10 and 100 µM *cis*-Cryptozepine-**2** enriched form (active isomer) was assessed on human M_1 and M_2 receptors expressed in Chinese hamster ovary (CHO) cells (see the **Experimental Section**).

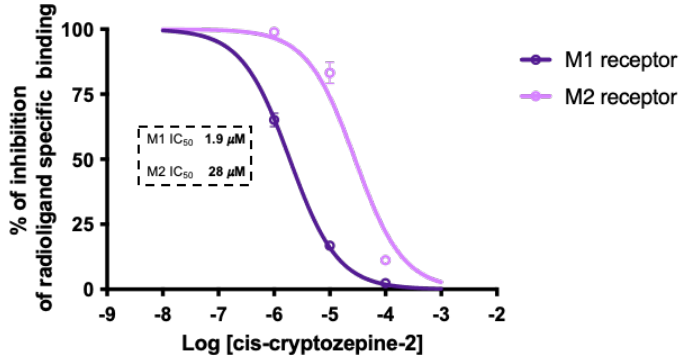

Figure S5.2. Inhibitory dose-response curves of *cis*-cryptozepine-2 on M1 (purple line) and M2 (pink line) receptors. The concentration-dependent inhibitory dose-curve data were plotted as percentage inhibition of radioligand specific binding (**Figure 3E**). The IC_{50} values determined for *cis*-cryptozepine-2 on M1 and M2 receptors are 1.9 and 28 μM, respectively. The curves were obtained by nonlinear regression analysis using GraphPad Prism.

6. *In vitro* calcium imaging experiments

6.1 Control experiments

In order to assess the significance of cryptozepine-2 and -3 (photo)responses in M1 mAChR expressing cells, further control experiments were performed in tsA201 cells without the transfection with M_1 receptor. No responses were observed after application of acetylcholine (ACh), cryptozepine-2 and 3, and under illumination at 460 nm, which excludes any response artifacts.

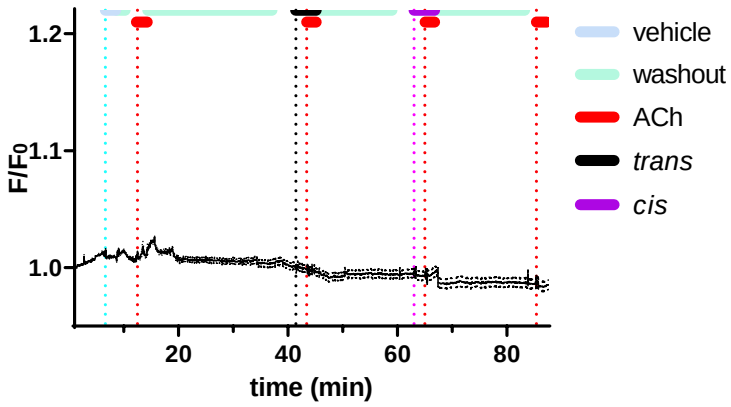

Figure S6.1.1. Control experiments for cryptozepine-2 with *in vitro* calcium imaging experiments in tsA201 cells without the presence of M1 receptor. No calcium oscillations were observed after application of ACh, cryptozepine-2 in the dark-adapted state (*trans*) and after 365 nm illumination (*cis*) (n = 50 cells). Error bars are ± SEM.

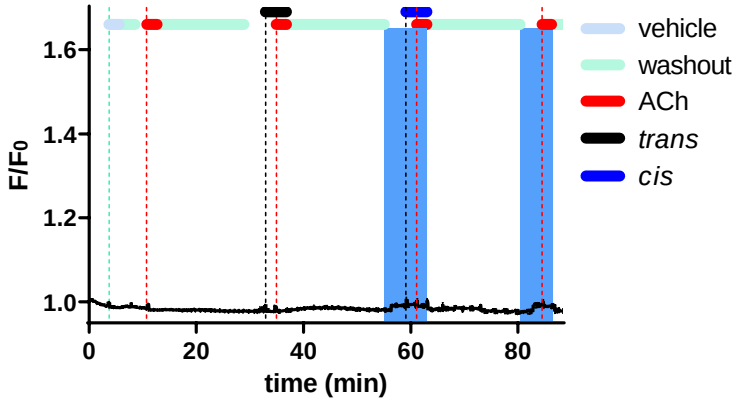

Figure S6.1.2. Control experiments for cryptozepine-3 with *in vitro* calcium imaging experiments in tsA201 cells without the presence of M1 receptor. No calcium oscillations were observed after application of ACh, cryptozepine-3 in the dark-adapted state (*trans*) and under 460 nm illumination (*cis*) (n = 50 cells). Error bars are ± SEM.

To validate our results, we performed calcium imaging recordings using the M_1 antagonist pirenzepine (PNZ) (Sigma-Aldrich). We used pirenzepine at decreasing concentrations ranging from 10 nM to 100 μM, 2 minutes prior to ACh application. As expected, at concentrations of 100 μM, 1μM and 100nM, we observed a significant inhibition of 89%, 85% and 52% of ACh-mediated calcium response respectively. However, the lowest concentration of PNZ (10 nM) had no significant effect.

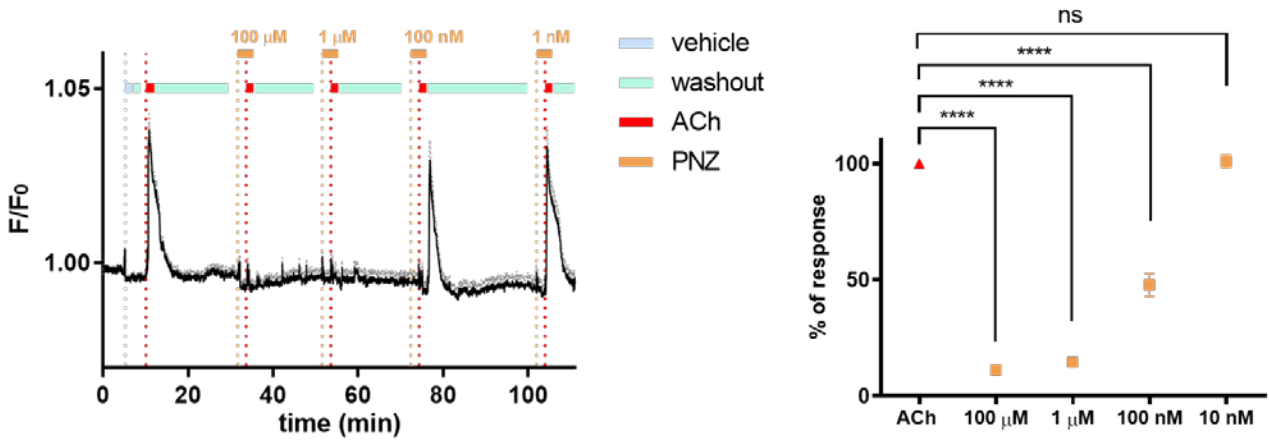

Figure S6.1.3. Pirenzepine (PNZ) antagonizes ACh-induced activation of M1 mAChRs. Real-time calcium imaging traces from HEK cells expressing M_1 mAChRs, which were loaded with the calcium indicator OGB-1 AM (10 μM). Pirenzepine (PNZ) was used at concentrations ranging from 10 nM to 100 μM. The cell responses to ACh (0.5 μM) were significantly reduced in the presence of PNZ (100 μM, 1 μM and 100 nM). However, cell responses were recovered at lowest concentration (10 nM). Standard Error of the mean (SEM) is in gray. Quantification results are presented in the right graph (n = 94 cells). The data were normalized over the maximum response obtained with 0.5 μM ACh and analyzed by the paired sample Wilcoxon signed rank test (p-value (***) < 0.001 (****) < 0.0001; GraphPad Prism 6. Error bars are ± SEM.

7. *Ex vivo* mice atria tissue experiments

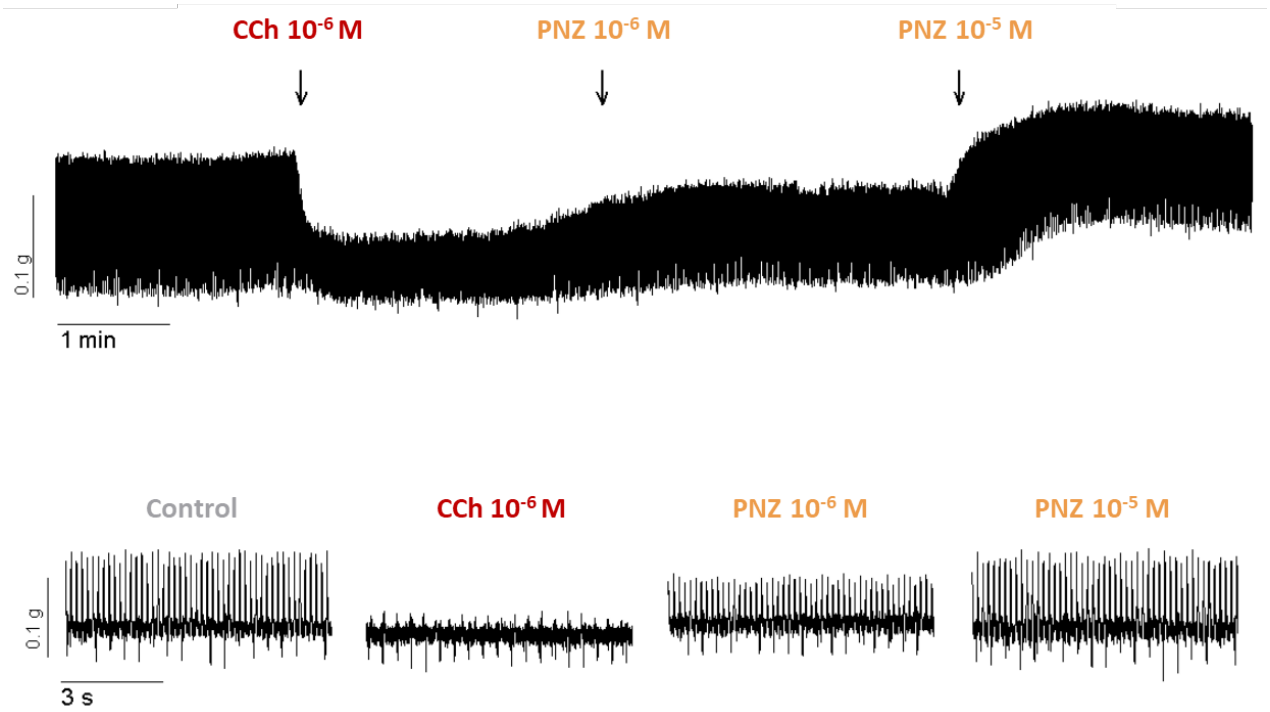

Figure S7.1. Representative profile of the measured heart rate of a mouse right atrium treated with pirenzepine. Spontaneous mechanical contractions were recorded as Control (ctrl). Carbachol (CCh) 10^{-6} M decreased both the amplitude and beats/min (bpm). The presence of pirenzepine (PNZ) (n = 6) concentration-dependently reversed the bradycardic effect of CCh 10^{-6}M.

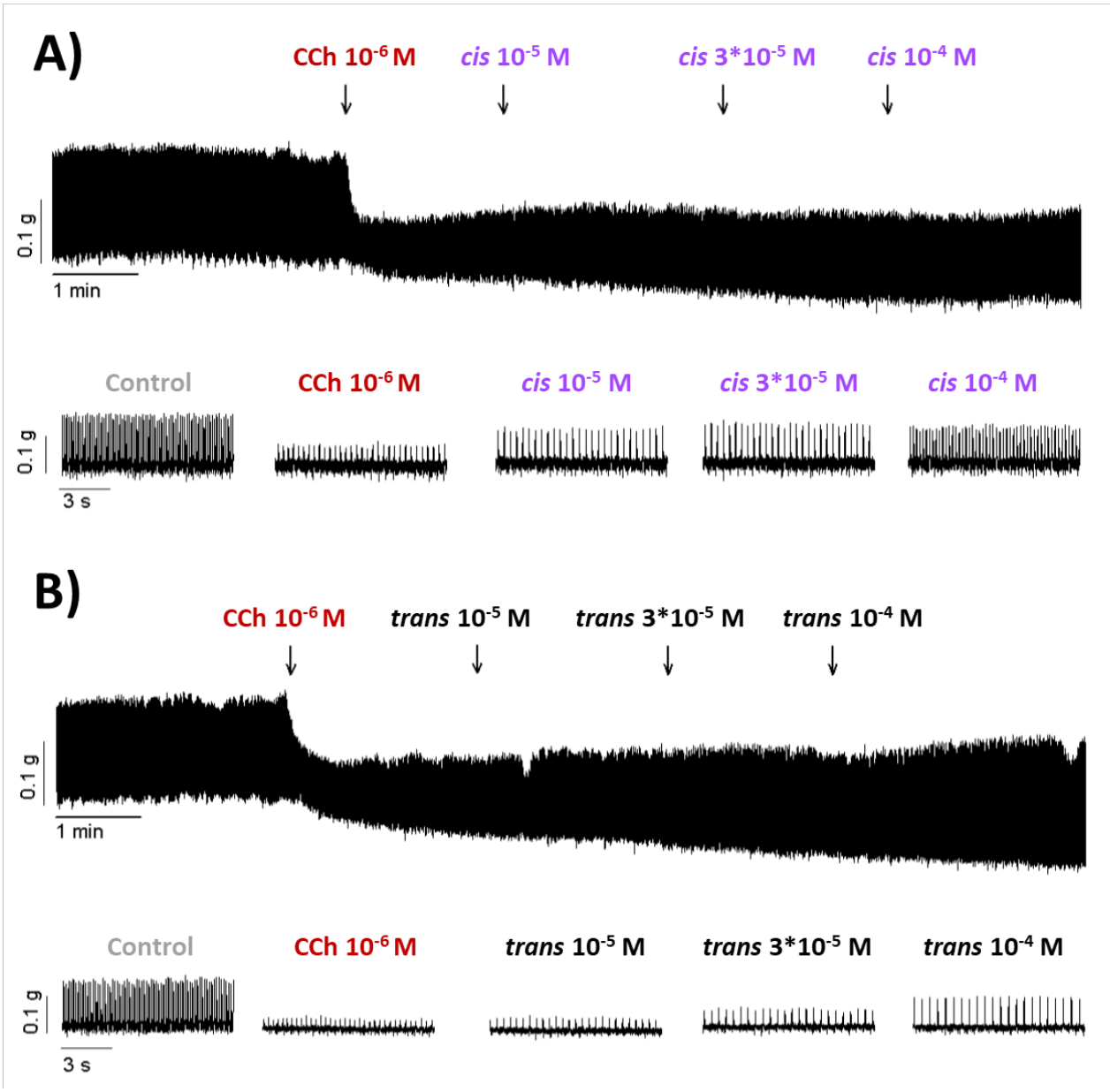

Figure S7.2. Representative profile of the measured heart rate of a mouse right atrium treated with cryptozepine-2. Spontaneous mechanical contractions were recorded as Control (ctrl). Carbachol (CCh) 10^{-6}M decreased both the amplitude and beats/min (bpm). The presence of *cis*-cyptozepine-2 (***cis***) (n = 2) concentration-dependently reversed the bradycardia induced by CCh 10^{-6}M (Panel **A**), in line with the pirenzepine effect. In contrast, *trans*-cryptozepine-2 (*trans*) (n =2) did not reserve CCh effect in terms of heartbeat frequency (n = 2) (Panel **B**).

8. Additional References

(1) Thal, D. M.; Sun, B.; Feng, D.; Nawaratne, V.; Leach, K.; Felder, C. C.; Bures, M. G.; Evans, D. A.; Weis, W. I.; Bachhawat, P.; Kobilka, T. S.; Sexton, P. M.; Kobilka, B. K.; Christopoulos, A. Crystal Structures of the M1 and M4 Muscarinic Acetylcholine Receptors. *Nature* **2016**, *531* (7594), 335–340. https://doi.org/10.1038/nature17188.

(2) Morris, G. M.; Huey, R.; Lindstrom, W.; Sanner, M. F.; Belew, R. K.; Goodsell, D. S.; Olson, A. J. AutoDock4 and AutoDockTools4: Automated Docking with Selective Receptor Flexibility. *J. Comput. Chem.* **2009**, *30* (16), 2785–2791. https://doi.org/10.1002/jcc.21256.

(3) Dallakyan, S.; Olson, A. J. Small-Molecule Library Screening by Docking with PyRx. In *Methods in molecular biology (Clifton, N.J.)*; 2015; Vol. 1263, pp 243–250. https://doi.org/10.1007/978-1-4939-2269-7_19.

(4) Lu, Z. L.; Saldanha, J. W.; Hulme, E. C. Transmembrane Domains 4 and 7 of the M1 Muscarinic Acetylcholine Receptor Are Critical for Ligand Binding and the Receptor Activation Switch. *J. Biol. Chem.* **2001**, *276* (36), 34098–34104. https://doi.org/10.1074/jbc.M104217200.

(5) Eberlein, W. G.; Engel, W. W.; Trummlitz, G.; Schmidt, G.; Hammer, R. Tricyclic Compounds as Selective Antimuscarinics. 2. Structure-Activity Relationships of M1 Selective Antimuscarinics Related to Pirenzepine. *J. Med. Chem.* **1988**, *31* (6), 1169–1174. https://doi.org/10.1021/jm00401a016.

(6) Murgolo, N. J.; Kozlowski, J.; Tice, M. A. B.; Hollinger, F. P.; Brown, J. E.; Zhou, G.; Taylor, L. A.; McQuade, R. D. The N4 Nitrogen of Pirenzepine Is Responsible for Selective Binding of the M1 Subtype Human Muscarinic Receptor. *Bioorganic Med. Chem. Lett.* **1996**, *6* (7), 785–788. https://doi.org/10.1016/0960-894X(96)00107-2.